



**HAL**  
open science

## Dynamic contributions of stratified groundwater to streams controls seasonal variations of streamwater transit times

Jean Marçais, Louis A Derry, Luca Guillaumot, Luc Aquilina, Jean-Raynald de Dreuzy

► **To cite this version:**

Jean Marçais, Louis A Derry, Luca Guillaumot, Luc Aquilina, Jean-Raynald de Dreuzy. Dynamic contributions of stratified groundwater to streams controls seasonal variations of streamwater transit times. *Water Resources Research*, In press, pp.e2021WR029659. 10.1029/2021wr029659 . insu-03579375v1

**HAL Id: insu-03579375**

**<https://insu.hal.science/insu-03579375v1>**

Submitted on 18 Feb 2022 (v1), last revised 30 Mar 2022 (v2)

**HAL** is a multi-disciplinary open access archive for the deposit and dissemination of scientific research documents, whether they are published or not. The documents may come from teaching and research institutions in France or abroad, or from public or private research centers.

L'archive ouverte pluridisciplinaire **HAL**, est destinée au dépôt et à la diffusion de documents scientifiques de niveau recherche, publiés ou non, émanant des établissements d'enseignement et de recherche français ou étrangers, des laboratoires publics ou privés.

# Dynamic contributions of stratified groundwater to streams controls seasonal variations of streamwater transit times

Jean Marçais<sup>1,2</sup>, Louis A. Derry<sup>3,2</sup>, Luca Guillaumot<sup>4,5</sup>, Luc Aquilina<sup>4</sup>,  
Jean-Raynald de Dreuzy<sup>4,6</sup>

<sup>1</sup>INRAE, UR Riverly, F-69625 Villeurbanne, France

<sup>2</sup>Institut de Physique du Globe de Paris, Université de Paris, CNRS, F-75005 Paris, France

<sup>3</sup>Department of Earth and Atmospheric Sciences, Cornell University, Ithaca, NY

<sup>4</sup>Univ Rennes, CNRS, Géosciences Rennes - UMR 6118, F-35000 Rennes, France

<sup>5</sup>International Institute for Applied Systems Analysis, Laxenburg, Austria

<sup>6</sup>Univ Rennes, CNRS, OSUR Observatoire des sciences de l'univers de Rennes - UMS 3343, F-35000  
Rennes, France

## Key Points:

- Hydraulic conductivity controls groundwater flow contributions to streams while porosity directly scales the streamwater mean transit times.
- Seasonal groundwater contributions to streams modulate the mean transit times dynamics from 6 years at high flows to 20 years at low flows.
- Stratified groundwater ages lead to a significant fraction (> 75 %) of old water to streamflow (>1 year).

---

Corresponding author: Jean Marçais, [jean.marcais@inrae.fr](mailto:jean.marcais@inrae.fr)

This article has been accepted for publication and undergone full peer review but has not been through the copyediting, typesetting, pagination and proofreading process, which may lead to differences between this version and the [Version of Record](#). Please cite this article as [doi: 10.1029/2021WR029659](https://doi.org/10.1029/2021WR029659).

This article is protected by copyright. All rights reserved.

## Abstract

Streamwater transit time distributions display a variable proportion of old waters ( $\geq 1$  yr). We hypothesize that the corresponding long transit times result from groundwater contributions to the stream and that seasonal streamwater transit time variations result from 1) the variable contributions of different flowpaths (overland flow, seepage flow and baseflow) and 2) the stratification of groundwater residence times. We develop a parsimonious model to capture the groundwater contribution to the stream discharge and its effect on transient transit times. Infiltration is partitioned according to the aquifer saturation between Boussinesq groundwater flow and overland flow. Time-variable transit time distributions are obtained with a new 2D particle tracking algorithm. Hydraulic conductivity, total and drainable porosities are calibrated by using discharge and CFC tracer data on a crystalline catchment located in Brittany (France). The calibrated models succeed in reproducing CFCs concentrations and discharge dynamics. The groundwater flow contribution to the stream is controlled by the aquifer hydraulic conductivity, while its age is controlled by the drainable and total porosities. Old groundwater ( $\geq 1$  yr) is the source for approximately 75 % of the streamflow with strong seasonal variations (between 40 and 95 %). Mean transit times are approximately 13 years, varying between 6 and 20 years, inversely proportional to the groundwater contribution. These seasonal variations are driven by the groundwater versus overland flow partitioning. The stratification of groundwater residence times in the aquifer plays a minor role in the streamwater transit times but is key for the transit time dynamics of the groundwater contribution to the stream.

## Plain Language Summary

Water entering a catchment as precipitation can take multiple paths with different transit times to the stream. While a significant fraction of water has short transit times (i.e. is “young”) when it reaches the stream, there is also an important contribution of “old” water with long transit times in the subsurface. The age distribution of this old component is important for understanding the resilience of watersheds to climate change, the behavior of persistent pollutants and chemical weathering processes. We developed a model, informed with discharge time series and atmospheric age tracer (CFCs), to constrain the age distribution in both groundwater and streamwater and how they vary seasonally. In our temperate test catchment with crystalline bedrock (Brittany, France), we find that the mean age of streamwater exiting the catchment is approximately 13 years, but varies seasonally from 6 to 20 years as the relative contributions of older groundwater and younger runoff change. Groundwater stratification further influences the mean age of the groundwater contribution arriving at the stream.

## 1 Introduction

Transit time is the time elapsed between the moment a water molecule enters a hydrological system (e.g. a catchment) and the moment it exits (e.g. through discharge) (Sprenger et al., 2019). This quantity is a fundamental descriptor of the hydrological fluxes and transport within the Critical Zone (Botter et al., 2020). Sampled streamwater, comprised of many water molecules with different transit times, reflects the diversity of flowpaths to the stream and its age distribution can provide information about Critical Zone structures (Kirchner et al., 2000, 2001; Brantley et al., 2017; Kuppel et al., 2020). This

64 distribution of transit times, though not directly observable, is a powerful integral quan-  
65 tity for understanding catchment-scale processes (Ameli et al., 2017; Gabrielli et al., 2018;  
66 Heidbüchel et al., 2020). It varies at different time scales, from the event to the seasonal  
67 and interannual time scales, reflecting the interplay between climatic variations and catch-  
68 ment structures as well as their impact on water resources at the catchment scale (Heidbüchel  
69 et al., 2013; Remondi et al., 2018, 2019). Characterizing streamwater transit time dis-  
70 tributions (TTDs) is therefore critical to define sustainable water use (Ferguson et al.,  
71 2020), evaluate climate change impacts on water resources (Maxwell et al., 2016; Fang  
72 et al., 2019), assess the effect of contaminant legacy (e.g. agricultural nutrient and pes-  
73 ticides) (van der Velde et al., 2010; Van Meter et al., 2016, 2018; Ehrhardt et al., 2019),  
74 as well as better understand Critical Zone evolution through weathering and erosion (Maher,  
75 2010; Maher & Druhan, 2014; Li et al., 2017; R. S. Anderson et al., 2019).

76 While the distribution of transit times is weighted toward young ages ( $\leq 1$  year)  
77 in most catchments (Jasechko et al., 2016; Benettin, Bailey, et al., 2017; Harman, 2014),  
78 it also includes a variable and difficult-to-constrain contribution from older water ( $\geq 1$   
79 year) investigated by only few studies (Stolp et al., 2010; Kaandorp et al., 2018; Visser  
80 et al., 2019). This old water fraction that has experienced a long transit time in the hy-  
81 drologic system may be a smaller component of stream fluxes (Gardner et al., 2011), but  
82 is critical to constrain for several reasons. These include but are not limited to the fol-  
83 lowing. 1) The resilience of surface water fluxes in the face of climate variability (drought,  
84 climate change) can depend heavily on the availability of old groundwater contributions  
85 to streamflow (Manning et al., 2012; Solder et al., 2016). 2) The recovery time scale of  
86 a watershed with persistent chemical pollutants can be alleviated by the old water con-  
87 tribution due to dilution or reactive processes (Aquilina et al., 2012; Pinay et al., 2015;  
88 Van Meter & Basu, 2017; Kolbe et al., 2019). 3) Chemical weathering (water-rock or water-  
89 regolith) reactions are often kinetically limited and water components with long reac-  
90 tion time scales are necessary to produce quasi-equilibrium solute and tracer composi-  
91 tions (Maher, 2011; Fernandez et al., 2021). Thus “older” water may be a smaller con-  
92 tributor to stream discharge but can have a disproportionate influence on weathering re-  
93 actions and streamwater quality (Frisbee et al., 2013). Predicting the future response  
94 of watersheds to anthropogenic climate forcing requires that we have an improved abil-  
95 ity to accurately model the old component of the distribution of watershed transit times  
96 and how that distribution varies in response to hydrologic and landscape forcing (Heidbüchel  
97 et al., 2012; Wilusz et al., 2017).

98 Here we focus on characterizing old streamwater ages ( $\geq 1$  year). We hypothesize  
99 that :

- 100 • old streamwater transit times result from the high contributions of subsurface aquifers  
101 and from strong groundwater flow residence time stratification (i.e. young ages  
102 at the top of the aquifer and old ages at the bottom, see Figure 1), tied to the hy-  
103 draulic properties of the aquifer (porosity, hydraulic conductivity);
- 104 • the dynamic partitioning of discharge between groundwater flows and overland flows  
105 explains the high seasonal variability of river discharge while the old component  
106 of the streamwater does not evolve much.

107 To assess the relevance of these two processes (i.e. stratification and partitioning)  
108 for old mean streamwater transit times and their seasonal variability, we could not use

109 previously developed families of transit time models. The first family of models spans  
 110 all the lumped representation of transit time distribution, from the simple lumped pa-  
 111 rameters models (Małozzewski & Zuber, 1982; Marçais et al., 2015) to more advanced  
 112 storage selection function approaches (Harman, 2014; Rinaldo et al., 2015; Benettin, Soulsby,  
 113 et al., 2017; Benettin & Bertuzzo, 2018; Nguyen et al., 2021). This type of models are  
 114 not appropriate here because they do not account for spatially explicit processes, which  
 115 limit their ability to investigate the controls regarding transit time distributions shapes  
 116 (Gauvain et al., 2021), as well as the impact of different flowpaths contributions to streams  
 117 on the development of transit time distributions. The second family of models encom-  
 118 passes detailed, spatially explicit process-based models such as Fatichi et al. (2016); X. Yang  
 119 et al. (2018); Therrien and Sudicky (1996); Kollet and Maxwell (2006); Camporese et  
 120 al. (2010). Their explicit description requires constraints on a number of parameters that  
 121 can be difficult to obtain in many circumstances, and whose calibration may not be unique.  
 122 Besides, due to their high computation requirements, systematic exploration of the vari-  
 123 ability of response of these models depending on different parameters sets and on main  
 124 processes represented are often not carried out (Putti & Paniconi, 2004; Paniconi & Putti,  
 125 2015). We therefore develop a novel intermediate model that represents what we hypoth-  
 126 esize are the key processes playing a first order role for characterizing old streamwater  
 127 ages and the proportion of old groundwater in streams.

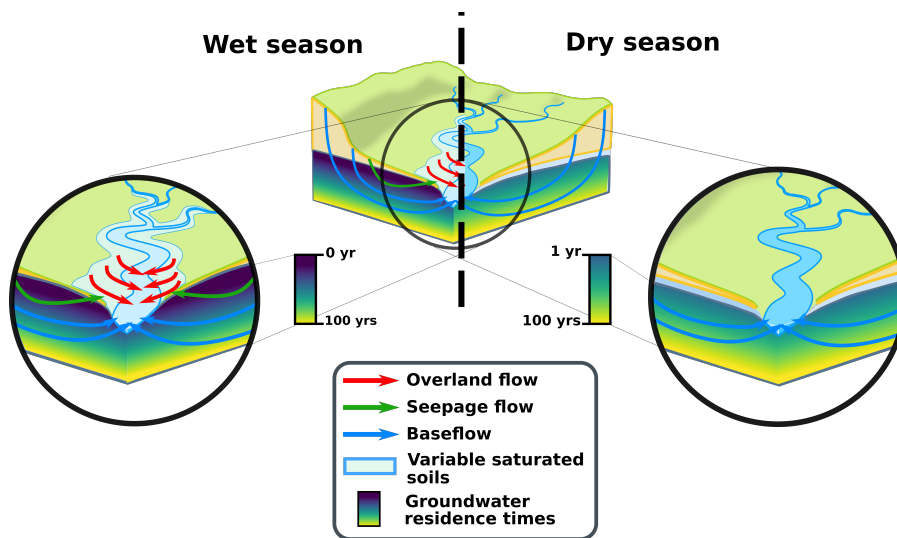


**Figure 1.** Sketch of the investigated processes. Where the water table intersects the land surface, it generates seepage flow (green arrows) and creates variable saturated areas that are responsive to precipitation (overland flow, red arrows). In the aquifer, groundwater flow is modeled with a Boussinesq formulation (blue arrows) adapted to take into account the groundwater residence time stratification (materialized by the colormap in the aquifer). Note the reduction of overland and seepage flows (red and green arrows) as well as the flush of young groundwater residence times from the wet (left side of the panel) to the dry season (right side of the panel) due to the small displacement of the water table.

128 We use a semi-explicit hillslope-scale approach that represents groundwater flows  
 129 inputs to streamwater with the vertically integrated approach proposed by Boussinesq  
 130 (Boussinesq, 1877; Dupuit, 1863). We modified the Boussinesq model to take into ac-

count the dynamic partitioning with the saturation excess overland flow and its fast routing to the stream network (S. P. Anderson et al., 1997; Freer et al., 2002; Blume & van Meerveld, 2015). We assume that the partitioning between groundwater flow and overland flow is controlled by the existence of seepage areas when the water table intersects the land surface (section 2.1, Marçais et al. (2017)). To represent the effect of the groundwater residence time stratification (Vogel, 1967; Kolbe et al., 2020), we develop a new transient and stratified transport model (section 2.2) adapted to the hillslope Boussinesq equations (Troch et al., 2003). Further, to overcome classic tracer resolution bias towards the young ages (Kirchner, 2016; Sprenger et al., 2019), we used CFC groundwater age data conjointly with monthly discharge time series to both quantify the groundwater contribution to stream and the transit time distribution dynamics (section 2.3). We test this approach on the 43 km<sup>2</sup> Guillec catchment of Brittany (France) as an example of shallow aquifers in crystalline regions (section 3). We discuss the relevance of such stratification and partitioning processes, the representativity of the calibrated catchment-scale parameters (hydraulic conductivity, drainable and total porosities), and the potential interest and limitations of the approach (section 4).

## 2 Flow model, transport model and study site

We recall the flux formalism relative to the hillslope storage Boussinesq equation modified to include overland flow generation (Marçais et al., 2017) (Figure 1). Advective transport is represented within a Lagrangian framework and solved with a particle tracking method accounting for the stratification of the solute transport in the aquifer and the routing of the saturation excess overland flow. It allows tracking of particle transit times and travel distances. Dispersive transport is added within the flow lines with an inverse Gaussian distribution. The model computes estimates of time-varying streamflows, transit time distributions of streamwater and residence time distributions of groundwater (Marçais, 2021) and these are compared to flow and transport data of the Guillec catchment (Brittany, France).

### 2.1 Flow model: partitioning groundwater from overland flow

Groundwater flows are based on a Boussinesq formalism for unconfined shallow aquifers (Troch et al., 2003; Paniconi et al., 2003) modified to account for saturation excess overland flow generation (Marçais et al., 2017). For a hillslope described by the width function  $\omega$ , the slope of the hillslope bedrock  $\theta$ , the aquifer thickness  $d$  and its hydraulic parameters, the drainable porosity  $\phi_d$  and the hydraulic conductivity  $k$  (Figure 2.A), groundwater flows draining to a stream are modeled by:

$$\left\{ \begin{array}{l} \frac{\partial S}{\partial t}(x, t) + q_S(x, t) = -\frac{\partial Q}{\partial x}(x, t) + N(t)\omega(x) \\ q_S(x, t) = \mathcal{G}\left(\frac{S(x, t)}{S_c(x)}\right) \mathcal{R}\left(-\frac{\partial Q}{\partial x}(x, t) + N(t)\omega(x)\right) \\ Q(x, t) = -\frac{kS(x, t)}{\phi_d} \left( \cos\theta \frac{\partial}{\partial x} \left( \frac{S}{\phi_d w} \right)(x, t) + \sin\theta \right) \\ S(x, t) = \phi_d \omega(x) h(x, t) \\ 0 \leq S(x, t) \leq S_c(x) = \phi_d \omega(x) d(x). \end{array} \right. \quad (1)$$

where  $t$  [T] is the time and  $x$  [L] the distance to the channel varying from 0 at the river to  $L$  at the water divide.  $S(x, t)$  [ $L^2$ ] is the groundwater storage per unit length  $dx$  varying from 0 to the maximum groundwater storage  $S_c(x)$  [ $L^2$ ],  $Q(x, t)$  [ $L^3/T$ ] is the integrated Boussinesq groundwater flux,  $N(t)$  [ $L/T$ ] is the infiltration time series and  $q_S(x, t)$  [ $L^2/T$ ] is the saturation excess overland flow generated per unit length  $dx$ .  $\mathcal{G}(u) = \mathcal{H}(u-1)$  and  $\mathcal{R}(u) = u \mathcal{H}(u)$  are two functionals depending on the relative saturation ( $S/S_c$ ) and flow balance ( $-\frac{\partial Q}{\partial x}(x, t) + N(t)\omega(x)$ ) based on the Heaviside step function  $\mathcal{H}$  to control the partition of incoming flux between water storage evolution and saturation excess overland flow (Figure 2.B, Marçais et al. (2017)).

The first equation of system 1 is the expression of the mass conservation for hillslope storage Boussinesq models (Troch et al., 2003). The second equation drives the local occurrence of saturation excess overland flow, when (1) groundwater storage saturates the whole aquifer column up to the surface  $\mathcal{G}(\frac{S(x,t)}{S_c(x)}) = 1$  (2) positive incoming flux locally occurs,  $-\frac{\partial Q}{\partial x}(x, t) + N(t)\omega(x) \geq 0$ . At these conditions, the functional  $\mathcal{R}$  is equivalent to the identity function (Figure 2.B) and  $q_S(x, t) = -\frac{\partial Q}{\partial x}(x, t) + N(t)\omega(x)$ . The third equation expresses the integrated groundwater flux  $Q(x, t)$  over the transect made up of a Darcy flow driven by the gradient of storage and of a gravity flow function of the bedrock slope. Fourth equation relates the groundwater storage  $S(x, t)$  to the hydraulic head  $h(x, t)$ . The last equation states that the groundwater storage  $S$  cannot be greater than  $S_c$ , since  $h(x, t)$  is limited by the maximum aquifer depth  $d(x)$ . Runoff occurrence thus appears to be both bottom-up controlled by the saturation of the aquifer, through the development of variably saturated source areas and top-down controlled by the occurrence of infiltration events.

To take into account the routing process of the saturation excess overland flow and seepage flow, from the hillslope surface to the river, we developed a 1D gravity driven routing model (Text S1). In this study, as we focus on monthly discharge and transit time distribution dynamics, we consider that the discharge in the river can be approximated by  $Q_{mod}(x, t) = Q(x, t) + \int_0^L q_S(x, t)dx$ , assuming that, at the monthly timescale, saturation excess overland flow can be considered to be routed to the stream on much smaller time scales (Musy & Higy, 2004).

## 2.2 Transport model: stratifying groundwater flowpaths

### 2.2.1 A 2D stratified, advective transport

2D advective transport is modeled within a Lagrangian framework defining the flow lines over the whole domain. Horizontal groundwater particles velocity  $v_x(x, t)$  directly derives from the Darcy flux  $Q$  integrated over the groundwater column (equation 3 of system 1), divided by the surface area of the porous section  $\phi_{tot}\omega h$ , where  $\phi_{tot}$  is the total aquifer porosity. Replacing the aquifer depth  $h$  by the groundwater storage  $S$  using the penultimate equation of system 1, we get :

$$v_x(x, t) = \frac{\phi_d}{\phi_{tot}} \frac{Q(x, t)}{S(x, t)} \quad (2)$$

By applying mass conservation principles to the hillslope Boussinesq equations, we retrieve the vertical component of the particle velocities  $v_z$  and obtain the following La-

207 grangian system of equations (see Appendix A):

$$208 \left\{ \begin{array}{l} S(x(t), t) \frac{dx}{dt}(t) = \frac{\phi_d}{\phi_{tot}} Q(x(t), t) \\ \frac{dz}{dt}(t) = -z(t) \frac{\phi_d}{\phi_{tot}} \left( \frac{d}{dx} \left( \frac{Q(x(t), t)}{S(x(t), t)} \right) + \frac{1}{w} \frac{dw}{dx} \frac{Q(x(t), t)}{S(x(t), t)} \right) \\ x(t_0) = x_0 \\ z(t_0) = z_0 = h(x_0, t_0) \end{array} \right. \quad (3)$$

209 where  $t_0$  is the initial time,  $\mathbf{x}_0 = (x_0, z_0)$  is the initial position of the flow line start-  
 210 ing at the water table and  $\mathbf{x}(t) = (x(t), z(t))$  is the 2D flow-line trajectory in the aquifer.  
 211 With this novel description, the vertical component of the velocity field is derived from  
 212 the horizontal velocity variations. Vertical transport of solutes is logically induced by  
 213 variations of velocity in the other horizontal directions.

214 The transport equation (3) is solved by a particle method where  $N_P = N_x N_t$  par-  
 215 ticles are injected for each of the  $N_t$  time steps at each of the  $N_x$  discretized elements.  
 216 Each particle is seeded at the top of the saturated zone and is flux-weighted according  
 217 to the intensity of the infiltration flux and to the relative area of the mesh cell (Figure  
 218 S1). Particles are injected in the aquifer where aquifer saturation remains below the land  
 219 surface, and at the surface otherwise.

220 For particles injected in the aquifer, this eventually leads to an aquifer stratifica-  
 221 tion where transit times increase with depth. Older particles are deeper in the aquifer  
 222 while the youngest ones, which have been just introduced through the most recent in-  
 223 filtration events, are above, closer to the water table (Figure 2). At each time  $t$ , parti-  
 224 cles crossing the groundwater boundaries (i.e. the water table and the imposed head bound-  
 225 ary condition at the river) go from the groundwater compartment directly to the seep-  
 226 age areas or to the river. They correspond respectively to the seepage flow and to the  
 227 baseflow (Figure 2). Their transit time is essentially equal to the time spent in the sub-  
 228 surface compartment  $\tau_{gw}(t)$ , as the transit time at the surface is much smaller. Parti-  
 229 cles injected at the surface are then assumed to have a transit time proportional to the  
 230 distance to the stream from where they have been injected:

$$231 \tau_{surf}(x, t) = \frac{x}{L_{sat}} \min_{1 \leq i \leq N(t)} \tau_{gw}^i(t) \quad (4)$$

232 where  $\tau_{surf}(x, t)$  is the transit time of the particles injected directly at the surface, at  
 233 a distance  $x$  from the river,  $L_{sat}(t)$  is the length of the saturated extension, and  $N(t)$   
 234 is the number of groundwater particles exiting at time  $t$ .

235 Due to the stratification obtained by the 2D trajectory description, seepage flow  
 236 is fed first by the youngest particles, which are at the top of the groundwater column.  
 237 Compared to other assumptions of full mixing over the water column, this method lo-  
 238 cates the streamline vertically, stratifies the transit times and correlates the depth of the  
 239 streamline to the distance of its origin. Deeper streamlines originate from farther away.  
 240 It has significant consequences on transit times. The youngest particles are the first to  
 241 exit at the onset of the seepage area. The oldest particles are the last to leave and exit  
 242 directly in the river. Overall the stratification increases the span of the transit time dis-  
 243 tribution. Equation (3) is solved in parallel with an implicit ode solver capable of man-  
 244 aging the presence of a singularity in the case where  $S(\mathbf{x}(t), t) = 0$ . This is achieved

245 with the variable time step and variable order ode15s MATLAB<sup>®</sup> solver (Shampine et  
 246 al., 1999). The numerical methods are validated by comparing the flux-based modeled  
 247 discharge  $Q_{mod}$  with the particular modeled discharge obtained by computing the par-  
 248 ticle flux reaching the stream at each time step (TextS2 and Figure S2). Results can be  
 249 expressed as particle trajectories.

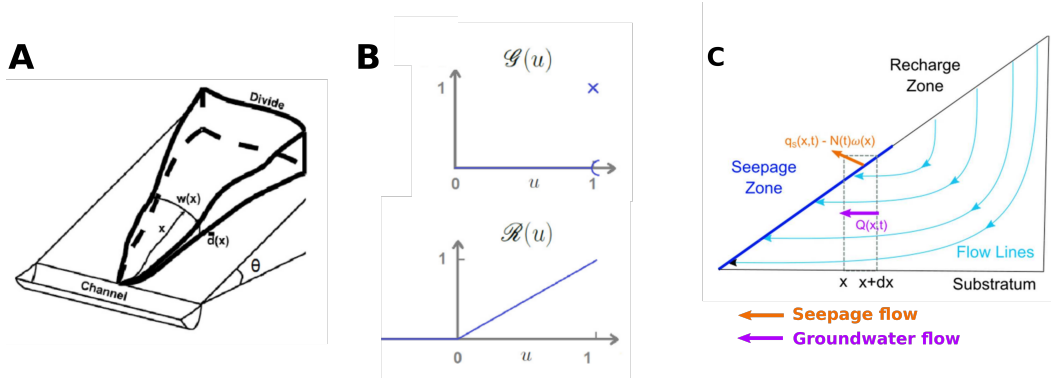


**Figure 2.** Sketch of A. the hillslope representation and geomorphologic variables ( $\omega(x)$ , the hillslope width,  $d(x)$ , the aquifer depth and  $\theta(x)$ , the hillslope bedrock slope), reproduced from Troch et al. (2003). B. the functions  $\mathcal{G}$  and  $\mathcal{R}$  used in the partitioning system of equations (1). C. the streamline organization. The stratification of the flow lines derived from the particle tracking method respects the conservation of mass laterally (in the direction modeled by the flux equation 1) and vertically through the premise of "no crossing" between streamlines. The strategy to retrieve seeping particles can be summarized as "last in, first out" for the particles, therefore suggesting a process-based interpretation for the preferential selection of young water discharged to the stream and to the seepage zone.

250 In the Boussinesq approach of groundwater flows, celerity (flux response to precipi-  
 251 tation) is dissociated from velocity (effective particle speed inside the aquifer) due to  
 252 three effects. First, the celerity response in time is only dictated by  $Q(x, t)$  while the ve-  
 253 locity response is driven by the ratio  $\frac{Q(x, t)}{S(x, t)}$ , meaning that the dynamics of stored drain-  
 254 able water also affect transport properties (Scaini et al., 2017). Second, the presence of  
 255 a non-linearity due to the water table intersection with the land surface creates a respon-  
 256 sive zone (the variable saturated areas) for flows, while the transport response is still pre-  
 257 dominantly controlled by the transit times of the particles travelling in the groundwa-  
 258 ter compartment. Third, it is the total amount of groundwater stored that effectively  
 259 conditions the particle velocity by modifying the Darcy velocity with the ratio  $\frac{\phi_d}{\phi_{tot}}$  (van  
 260 Verseveld et al., 2017). In this model, these three effects contribute to dissociate celer-  
 261 ity from velocity (McDonnell & Beven, 2014; McDonnell, 2017).

### 262 *2.2.2 A longitudinal advective-dispersive transport scheme to model time* 263 *variable residence time and transit time distributions*

264 The numerical scheme introduced in the previous section corresponds to the 2D  
 265 purely advective transport of a solute without any diffusion or dispersion. We introduce  
 266 longitudinal diffusive and dispersive processes in the aquifer by considering that trans-

port within each flow line can be modeled by an inverse Gaussian distribution accounting both for advective and diffusive/dispersive processes (Engdahl & Maxwell, 2014; Kirchner et al., 2001; de Marsily, 1986) (Text S3 and Figure S3). Dispersive and diffusive processes transversal to the flow lines are neglected because it is considered one order smaller than longitudinal dispersivity (de Marsily, 1986) and of second-order effects in such uniform media (de Dreuzy et al., 2007). For each particle with an age  $\tau$  (which can be considered as a transit time or as a residence time depending on the medium sampled, stream or catchment), we obtain the following expressions for the distribution of transit times  $p(t, \tau)$ :

$$\begin{cases} p(t, \tau) = \sqrt{\frac{25\tau}{4\pi t^3}} \exp\left(-\frac{25(t-\tau)^2}{4\tau t}\right) & \text{if } t \geq 0 \\ p(t, \tau) = 0 & \text{if } t < 0 \end{cases} \quad (5)$$

The residence time distribution at time  $t$  can be derived from the residence time of all the particles  $k$  located in the aquifer and at the surface. The transit time distribution at time  $t$  is defined from the transit time of the particles  $i$  reaching the river between  $t$  and  $t+\Delta t$ . In both cases, the distribution of times is obtained by summing up the inverse Gaussian distributions centered on their individual traveling time  $\tau^i$  in the aquifer and at the surface. Each of these inverse Gaussian distribution is weighted by the water volume associated to the particle. This results in synthetic, physically-based transient residence time distributions  $p_S(t, \tau)$  and transit time distributions  $p_Q(t, \tau)$ .

### 2.3 Guillec catchment: field data and modeling strategy

To illustrate the value of this modeling approach, we assessed its relevance on the Guillec catchment located in western Brittany (France). The Guillec catchment has a relatively limited size (43 km<sup>2</sup>). Discharge and CFC data are available. The Guillec catchment is characterized by an oceanic temperate climate with average precipitation of around 1000 mm/yr and real evapotranspiration approximately equal to 600 mm/yr. Its geology is crystalline, mainly granitic, though some siliclastic sedimentary materials are present in the fluvial system due to the weathering of the crystalline bedrock. Topographic gradients are relatively limited with altitudes ranging between 7 m and 125 m (Figure 3).

#### 2.3.1 Flux data: monitored discharge and modeled infiltration data

Daily discharge time series are available over 54 years at the catchment outlet. With the objective to analyze the interannual and seasonal fluctuations of discharge and time-varying transit time distributions, the monthly average of this time series is derived. Input forcings for our modeling strategy come from the SURFEX land surface model (Le Moigne et al., 2020) seeded with SAFRAN atmospheric reanalysis (Vidal et al., 2010). SAFRAN provides precipitation and energy atmospheric forcings over France at the unified national scale (8x8 km<sup>2</sup> grid) (Quintana-Seguí et al., 2008). The SURFEX land surface model computes water and energy budgets in the soil compartment and produces precipitation, real evapotranspiration, runoff (shallow runoff) and drainage (deep infiltration) on the same national grid scale (Boone et al., 2017). To stick to our modeling framework, we summed runoff and drainage time series to provide a proper infiltration time series as the model itself spatially resolves the partitioning between infiltration excess overland flow and recharge (Marçais et al., 2017).

### 308 *2.3.2 Transport data: sampling and interpretation of CFCs*

309 Depending on the timescale of interest, an appropriate age tracer has to be cho-  
310 sen for groundwater dating (Suckow, 2014; Kazemi et al., 2006). Previous modeling stud-  
311 ies in Brittany have estimated the mean streamwater transit times to be approximately  
312 5 years to 7 years (Martin et al., 2006; Mougin et al., 2015). Groundwater mean resi-  
313 dence times, which have been evaluated from CFC sampling in aquifers, show an older  
314 range, between 25 years (Marçais et al., 2018; Roques et al., 2014; Ayraud et al., 2008)  
315 and 50 years (Kolbe et al., 2016). Groundwater inputs to streams are significant, from  
316 30 % to 60 % of the stream discharge (Clément et al., 2003; Mougin et al., 2002, 2008;  
317 Aquilina et al., 2012). A first-order analysis shows apparent inconsistencies between these  
318 observations at least when they are compared to regional scale estimates, as a 50 % in-  
319 put of 25 year old groundwater to streams would lead to streamwater mean transit times  
320 of at least 12.5 years. As we are interested in understanding the contribution and age  
321 of groundwater to the Guillec river, we chose CFCs to date groundwater because CFC  
322 ages are sensitive to time scales of years to decades.

323 CFCs are assumed to be in equilibrium with the atmosphere in the unsaturated  
324 zone, provided that the water table is not too deep (typically not more than 5m)(Engesgaard  
325 et al., 2004), which is generally the case for Brittany (Mougin et al., 2004; Kolbe et al.,  
326 2016). Once the infiltrating water recharges the aquifer, it becomes isolated from the at-  
327 mosphere, with the dissolved concentration equilibrated with the atmospheric concen-  
328 tration at the time of isolation. CFCs are then assumed to be transported conservatively  
329 in the aquifer. For this analysis, we sampled the two wells shown as violet circles on Fig-  
330 ure 3A and the Guillec river close to its outlet (blue triangle). We calibrated the trans-  
331 port model on these three CFCs samples. Aerobic conditions prevent CFC degradation  
332 (Dunkle et al., 1993; Kolbe et al., 2020). In any case, exchanges between the samples and  
333 the atmosphere have been minimized, by sampling far from the river re-aeration zones  
334 and at the very bottom of the water column (Vautier et al., 2020; Guillaumot et al., 2021).  
335 The two wells were chosen because they are known to be located just upstream of well-  
336 identified springs. Sampled waters are thus confirmed to characterize the contribution  
337 of the aquifer to the stream. In the river, we sampled CFCs at the end of the low flow  
338 period in October to ensure both significant river depth and a majority of streamwater  
339 coming from the aquifer.

340 CFCs were analyzed at the CONDATE Eau facility of the University of Rennes,  
341 France (OSUR laboratory) (Ayraud et al., 2008; Labasque et al., 2014). CFC-11 and CFC-  
342 113 concentrations were found to be consistent with each other and were retained as mod-  
343 eling targets, except one contaminated CFC-11 sample (Table S1). In contrast, most CFC-  
344 12 concentrations appeared to be contaminated as the values were well above the max-  
345 imum atmospheric concentration ever recorded.

### 346 *2.3.3 Topographic data: an equivalent hillslope representation*

347 The hillslope model has been derived on the basis of the topographically defined  
348 catchment from the gauging station at the outlet (Figure 3A). SRTM data (Farr et al.,  
349 2007) were analyzed with the topotoolbox package (Schwanghart & Scherler, 2014) un-  
350 der the assumption that the hydrological and hydrogeological catchments correspond (Reggiani  
351 et al., 1998; Reggiani & Schellekens, 2003; Haitjema & Mitchell-Bruker, 2005; Gleeson  
352 & Manning, 2008). This assumption is generally appropriate in Brittany where limited

353 weathering of the crystalline bedrocks and low topographical gradients preclude the ex-  
 354 istence of significant regional groundwater circulation (Kolbe et al., 2016). We chose to  
 355 rely on a representation of the catchment based on an equivalent hillslope representa-  
 356 tion characterized by its relative elevation to the river (Loritz et al., 2017; Reggiani &  
 357 Schellekens, 2003). This equivalent hillslope is obtained by aggregating the cells of the  
 358 DEM in a 1D representation according to their distance to the river in the DEM (Fig-  
 359 ure 3B and C). The slope of its surface is relatively limited to be around 2.5 %. The 2D  
 360 DEM-based analysis gives the width function and the mean elevation function at the scale  
 361 of the catchment. Assuming a flat bedrock located at the same elevation as the river out-  
 362 let (L’vovich, 1979), the width and elevation functions characterize the storage capac-  
 363 ity of the catchment  $S_{tot}$  (which we assumed to be mainly located in its shallow aquifer)  
 364 as a function of the distance to the stream:  $S_{tot}(x, t) = \phi_{tot} \omega(x) d(x)$ .

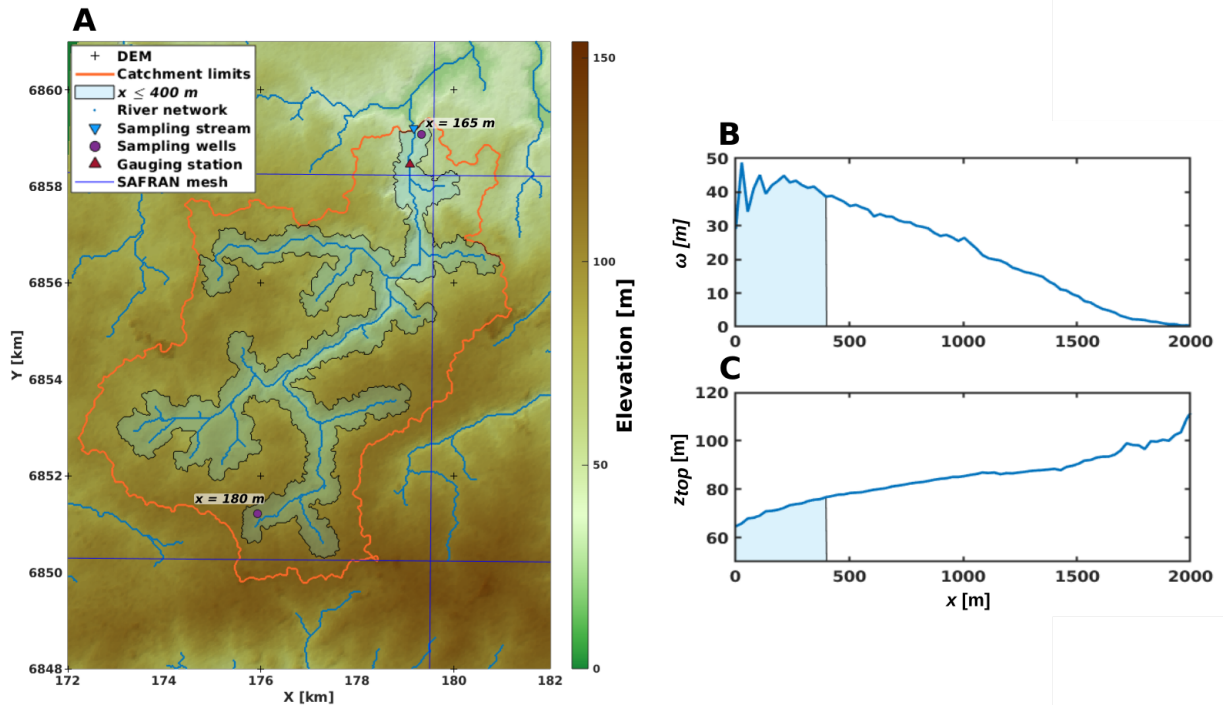


**Figure 3.** (A) 2D representation of the topography of the Guillec catchment with the sampling locations indicated as circles and triangles. The distance of the sampled locations to the river are indicated in black. The gridding mesh used to retrieve infiltration time series from the SURFEX model is superimposed in blue. (B) Width function  $\omega(x)$  and (C) elevation function  $z_{top}(x)$  of the equivalent hillslope characterizing the repartition of the catchment area as a function of the distance  $x$  to the stream. To illustrate the aggregation strategy, we highlight the elevation and the width of the equivalent hillslope in pale blue for a distance to the stream smaller than 400 m. Corresponding DEM cells are highlighted with the same color in (A).

### 365 2.3.4 Model calibration

366 The model has 3 parameters to calibrate, which are the bedrock hydraulic conduc-  
 367 tivity  $k$ , the bedrock drainable porosity  $\phi_d$  and the bedrock total porosity  $\phi_{tot}$ . Accord-  
 368 ing to the available data, our strategy is first to select the most promising flow models  
 369 defined by their hydraulic conductivity  $k$  and their drainable porosity  $\phi_d$  with the monthly  
 370 discharge observations and second to determine the total aquifer porosity  $\phi_{tot}$  with the  
 371 sampled CFCs measurements.

372 Flows are modeled by the methods given in section 2.1 with a finely discretized mesh  
 373 of 500 cells (4m wide). We calibrated the flow model parameters, i. e. the aquifer hy-  
 374 draulic conductivity  $k$  and the drainable porosity  $\phi_d$ , on the monthly discharge time se-  
 375 ries. We ran 25,000 simulations with a Monte Carlo sampling method,  $k$  in the range  
 376  $[10^{-8}, 10^{-4}]$  m/s and  $\phi_d$  in the range  $[0.005, 0.5]$ . The goodness of fit is assessed by the  
 377 Kling-Gupta efficiency (KGE) (Gupta et al., 2009). KGE increases for better models and  
 378 reaches 1 for a perfect fit.

379 We selected the 39 best simulations giving the highest KGE values and ran the advective-  
 380 dispersive transport on them for different  $\phi_{tot}$  values in  $[\phi_d, 0.5]$ . This resulted in 147  
 381 transport simulations on which CFC-11 and CFC-113 concentrations ( $C_{CFC}^{mod}(t_s, x)$  ex-  
 382 pressed in equivalent to atmospheric concentration, where  $t_s$  is the sampling time and  
 383  $x$  is the distance of the sampling location to the river) are estimated in the river and in  
 384 the wells, under the assumption of no atmospheric contamination, with the classic con-  
 385 volution equation (Marçais et al., 2015). We then calibrated the hillslope transport model  
 386 on the CFC concentrations, by minimizing the following objective function:

$$387 \Theta(k, \phi_d, \phi_{tot}) = 1 - \frac{1}{6} \left( \frac{\sum_{i=1}^3 |C_{CFC11_i}^{mod}(x_i) - C_{CFC11_i}^{obs}(x_i)|}{\sum_{i=1}^3 |C_{CFC11_i}^{obs}(x_i)|} \right. \\ \left. + \frac{\sum_{i=1}^3 |C_{CFC113_i}^{mod}(x_i) - C_{CFC113_i}^{obs}(x_i)|}{\sum_{i=1}^3 |C_{CFC113_i}^{obs}(x_i)|} \right) \quad (6)$$

388 Like the *KGE* indicator,  $\Theta$  gets close to 1 for perfect fits.

## 389 3 Results

390 We present the calibration results and the capacity of the discharge and CFCs data  
 391 to constrain the aquifer hydraulic parameters (section 3.1). The calibrated models show  
 392 the control of the streamwater mean transit times by the groundwater contribution (sec-  
 393 tion 3.2) and illustrate its seasonal evolution with the dynamic partitioning of the over-  
 394 land flow, seepage flow and baseflow (section 3.3).

### 395 3.1 Calibration of the aquifer hydraulic parameters

#### 396 3.1.1 Calibration of the hydraulic conductivity by discharge data

397 Hydraulic conductivity  $k$  and drainable porosity  $\phi_d$  are evaluated by comparing the  
 398 observed and simulated discharge data at the Guillec catchment outlet according to the  
 399 *KGE* metric (Figures 4.A, S4, S5 and Text S4). The modeled discharge is highly sen-  
 400 sitive to both  $k$  and  $\phi_d$  with *KGE* values broadly ranging between 0.040 and 0.82. The  
 401 local maximum values of *KGE* are underlined by the dashed red curve and cover a wide

402 range of  $k$  and  $\phi_d$  values organized around two trends respectively horizontal and ver-  
 403 tical (Figures 4.A, S6 and Text S5). For the vertical trend,  $k$  is well constrained around  
 404  $10^{-5}$  m/s while  $\phi_d$  broadly varies between 2 % and 47 %. For the horizontal trend,  $\phi_d$   
 405 is smaller around 1 % while  $k$  varies between  $10^{-5}$  m/s and  $9 \times 10^{-5}$  m/s. It shows that  
 406 discharge data constrain the hydraulic conductivities within less than one order of mag-  
 407 nitude (from  $1 \times 10^{-5}$  m/s to  $9 \times 10^{-5}$  m/s) out of the 4 orders of magnitude explored  
 408 (from  $10^{-8}$  m/s to  $10^{-4}$  m/s). The drainable porosity  $\phi_d$  is however poorly constrained  
 409 with the best simulations spanning almost all the explored range, from 0.6 % to 47 %.  
 410 At this stage, We select the 39 sets of parameters ( $k, \phi_d$ ) giving the best  $KGE$  values (i.e.  
 411  $KGE \geq 0.8$ , indicated by dots on Figure 4.A).

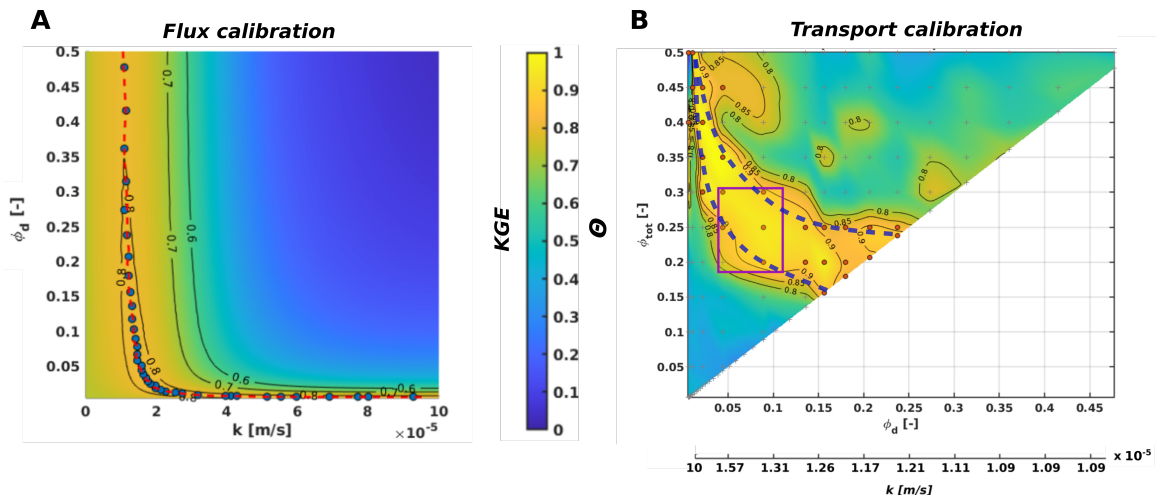


**Figure 4.** A.  $KGE$  calibration performance on discharge data displayed for the 25 000 simulations sampling the  $(k, \phi_d)$  parameter space. The dotted red curve indicates the location of the local maxima joining the 39 best models retained for the analysis (blue dots). B.  $\Theta$  calibration performance on CFCs data (6) in the  $(\phi_d, \phi_{tot})$  space. Orange circles represent the 28 best transport models. Dashed blue lines materialize the constrained zone in the  $(\phi_d, \phi_{tot})$  map. The purple rectangle further restrains the acceptable values within the range of values previously reported in the literature for the same type of lithologies (section 4.1). In the right figure, values of the hydraulic conductivity  $k$  corresponding to the drainable porosity  $\phi_d$  (obtained from the calibration of the discharge data, section 3.1) are represented on the lower scale (scale is not linear).

### 412 3.1.2 Calibration of drainable and total porosities by CFCs data

413 Starting from the 39 best flow models obtained with the previously identified  $(k,$   
 414  $\phi_d)$  sets, we defined 147 transport models with different values of  $\phi_{tot}$  to explore the pa-  
 415 rameter space defined by  $\phi_{tot} \geq \phi_d$ . We assessed the agreement between modeled and  
 416 sampled CFC concentrations with the function  $\Theta$  (equation 6 and Figure S7). Results  
 417 show that a close match is obtained for 28 of the 147 models with values of  $\Theta$  greater  
 418 than 0.8 defining a characteristic zone of acceptance in the  $(\phi_d, \phi_{tot})$  space (Figure 4.B).  
 419 By construction, the 28 models match both the sampled CFC concentrations and the  
 420 seasonal discharge variations.

421  $\phi_d$  and  $\phi_{tot}$  are partly constrained by CFC data (dashed blue lines on Figure 4.B),  
 422 while they were not by the discharge data. Admissible  $\phi_d$  and  $\phi_{tot}$  lead to streamwater  
 423 mean transit times equal to  $13 \pm 2$  years (Figures 5.B, S8 and S9). Any decrease of the  
 424 drainable porosity  $\phi_d$  is balanced by some increase of the total porosity  $\phi_{tot}$  to compen-  
 425 sate the speed up of the drainable flowpaths by some additional delay in the immobile  
 426 porosity ( $\phi_{tot} - \phi_d$ ).  $\phi_d$  and  $\phi_{tot}$  do not however have exactly the same effect.  $\phi_d$  mod-  
 427 ifies the speed of the drainable flowpaths, the dynamical storage of the aquifer and its  
 428 seasonal amplitude as well as the water table intersection with the topography and its  
 429 dynamic. In contrast,  $\phi_{tot}$  more directly scales the transit times (equation 3) through  
 430 a simple linear dependency, which clearly appears at steady state (Text S6 and Figure  
 431 S8).

### 432 3.2 Controls of streamwater mean transit times by groundwater con- 433 tributions

434 The contribution of groundwater to the streams is characterized by the Ground-  
 435 water Index. The Groundwater Index, abbreviated GWI, is defined as the proportion  
 436 of baseflow and seepage flow to the streamflow. It is on average equal to 75 % with a lim-  
 437 ited variability among the 39 best models ( $\pm 14$  %, Figure 5.A). When it reaches the stream,  
 438 groundwater is on average  $17 \pm 3.5$  years old (Figure 5.B). As a result, streamwaters are  
 439 relatively old with a mean transit time of 13 years ( $\approx 17 \times 0.75$ ) assuming that over-  
 440 land flows are less than 1 year old and intervene mostly through a dilution effect. Even  
 441 in the wet season when its contribution is reduced, groundwater still amounts to 40 %  
 442 of the stream discharge, explaining why streamwater transit times remain "old" ( $\approx 6.6$   
 443 years old).

444 Resulting from the Boussinesq response and from the seasonal water table inter-  
 445 section with the topography, GWI, the groundwater contributions to the stream varies  
 446 significantly throughout the year. GWI decreases from 0.98 at early low flows (August),  
 447 when streams are almost exclusively fed by aquifers, to 0.39 at early high flows (Decem-  
 448 ber), when precipitation and saturated areas are maximal (Figure 5.A). The streamwa-  
 449 ter mean transit time ( $mTT$ ) displays similar variations with a time lag of 1-2 months,  
 450 from 20 years at late low flows (October) to 6.5 years at the late high flow season (Febru-  
 451 ary) (Figure 5.B). The mean transit time of the groundwater contribution to the stream  
 452 ( $mTT_{gw}$ ) is further delayed by one month ( $mTT_{gw} \in [14.5, 33]$  years). This is because  
 453 deeper compartments of the catchment have a delayed response compared to the shal-  
 454 lower compartments.  $mTT_{gw}$  also displays an increased variability between the calibrated  
 455 models ( $\pm 3.5$  years for  $mTT_{gw}$  to compare with  $\pm 1.7$  years for the  $mTT$ ).

456 This shows that the groundwater contribution characterized by GWI, which is con-  
 457 trolled by the aquifer hydraulic conductivity  $k$  (section 3.1.1), itself controls the seasonal  
 458 dynamics of streamwater mean transit times  $mTT$ . Below, we further investigate the ef-  
 459 fect of flowpath decomposition on the full transit time distribution (TTD) and its sea-  
 460 sonal variations.

### 461 3.3 Structure of the Transit Time Distributions as revealed by the flow- 462 path organization

463 The decomposition of the transit time distribution in these three flowpath compo-  
 464 nents (overland flow, seepage flow and baseflow) shows how the spatial stratification of

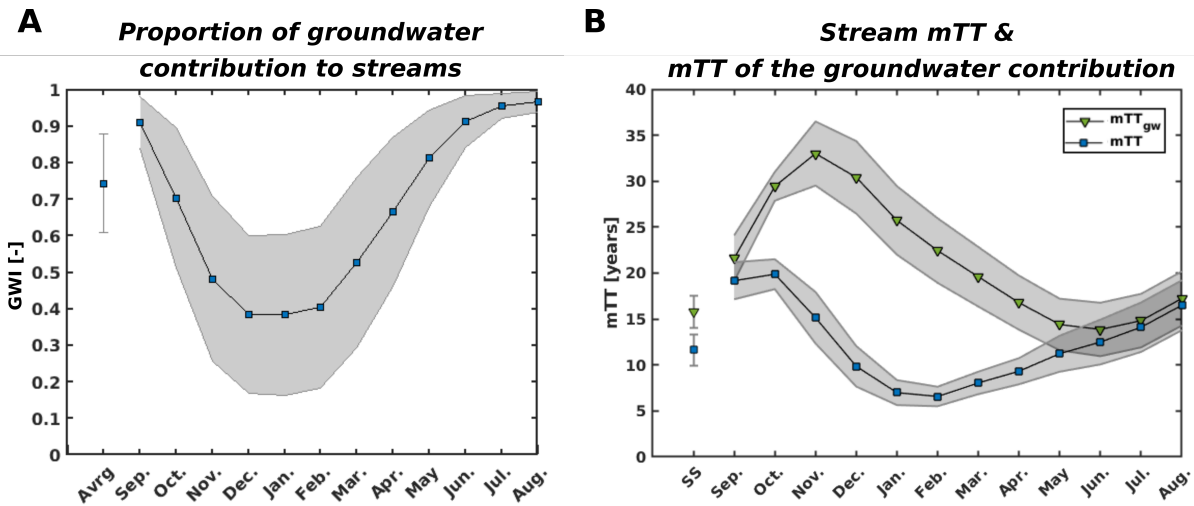


**Figure 5.** Modeled interannual monthly variations of A. the proportion of groundwater contributions to stream characterized by the Groundwater Index GWI and B. the streamwater mean transit times ( $mTT$ , squares) and mean transit times of the groundwater contribution to stream ( $mTT_{gw}$ , triangles). Note how the contribution of the aquifer is delayed compared to the river signal. The maximum  $mTT_{gw}$  is reached in November, one month later than  $mTT$  (maximum attained in October). The shaded area marks the standard deviation obtained with the 28 best transport models (out of 147 transport models). First points and error bars on the left labeled "Avrg" and "SS" stand respectively for the annual average and for the steady state value.

465 the flowpaths is translated in the time domain both in low flow and high flow periods  
 466 (Figure 6.A). Overland flows have the fastest times centered on one month (0.1 year) (red  
 467 curves). Seepage flows have an intermediate timescale centered on one year (green curves).  
 468 This timescale of one year reflects the seasonal seepage front development at the top of  
 469 the aquifer composed of groundwater with a residence time less than one year since it  
 470 is flushed every year. Third, the baseflow contribution has the oldest transit times with  
 471 an average timescale of 10 to 30 years depending on the season (blue curves).

472 Differences in the TTD decomposition between seasons (at high flow vs low flow)  
 473 lead to some counterintuitive results. At high flows (curves indicated by diamonds), the  
 474 transit times of the overland and seepage flows are surprisingly slightly longer than at  
 475 low flows. It results from the development of the seepage zone and reflects the fact that  
 476 runoff occurs from farther away from the river on the hillslope increasing the mean transit  
 477 time of overland flowpaths to the river. With receding seepage (crosses), flowpaths  
 478 emerging in the seepage zone become shorter by occurring closer to the stream. Similar  
 479 conclusions have been drawn by Wilusz et al. (2020). More intuitively, baseflow con-  
 480 tribution is older at low flows as it comes from deeper older compartments due to the  
 481 groundwater age stratification. Interestingly, the transit time distributions of the base-  
 482 flow contribution is the most sensitive to seasonal variations with transit timescales sig-  
 483 nificantly shifted from high flow (10 years) to low flow (30 years), in line with the  $mTT_{gw}$   
 484 seasonal variations (triangles in Figure 5.B).

485 However, we observe that the large seasonal mean transit time variations (squares  
 486 in Figure 5.B) do not result from the intrinsic  $mTT$  variability of the different flowpath

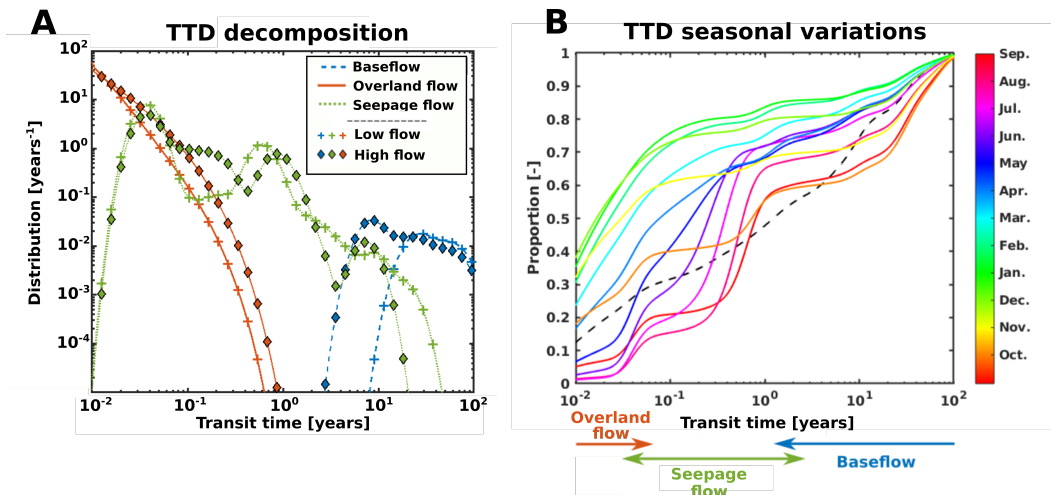


**Figure 6.** A. TTD decomposition in the streamflow components illustrated by Figure 1: overland flow (red solid lines), seepage flow (green dotted lines) and baseflow (blue dashed lines). TTDs are given at low flows in September 2016 (crosses) and at high flows in February 2017 (diamonds). B. Interannual averaged seasonal cumulative TTDs. During the wet season, the proportion of young water in the river increases significantly. The black dotted line represents the steady state transit time distribution. Transport simulation were obtained for  $k = 1.6 \times 10^{-5}$  m/s,  $\phi_d = 4\%$  and  $\phi_{tot} = 25\%$ . Note the well-separated characteristics transit times of the three flow components on both figures.

487 components (overland flow, seepage flow or deep flow), but rather from the time-varying  
 488 respective contribution of these fluxes to the stream discharge, in accordance with pre-  
 489 vious studies carried with the SAS framework (Rodríguez & Klaus, 2019; Wilusz et al.,  
 490 2020). The seasonal variations of the cumulative transit time distributions shown by Fig-  
 491 ure 6.B confirm this. On this plot, the lines of the cumulative TTDs indeed display sharp  
 492 increases at specific transit timescales illustrating shifts in the relative proportion of these  
 493 flowpaths.

## 494 4 Discussion

### 495 4.1 Complementarity of discharge and CFCs data informs catchment 496 scale hydrological properties and processes

497 Discharge data turn out to illuminate hydraulic conductivity at the catchment scale  
 498 by constraining its range to less than one order of magnitude between  $10^{-5}$  m/s and  $9 \times$   
 499  $10^{-5}$  m/s. Such values of hydraulic conductivities are consistent with previous ranges  
 500 of hydraulic conductivities and transmissivities obtained at comparable scales for the crys-  
 501 talline basements of Brittany as shown by Table 1 (Conan et al., 2003; Grimaldi et al.,  
 502 2009; Molenat, 1999; Clément et al., 2003; Legchenko et al., 2004; Martin et al., 2006;  
 503 Kolbe et al., 2016; Leray et al., 2012; Le Borgne et al., 2006; Roques et al., 2014). The  
 504 limited range of estimated hydraulic conductivity and the agreement with independently  
 505 derived values show that this method adequately constrains hydraulic conductivities at  
 506 the catchment scale. It offers a complementary approach to the classic analysis of reces-  
 507 sion first introduced by Brutsaert and Nieber (1977), which requires essential but difficult-

508 to-assess assumptions for extracting the baseflow contribution (Wittenberg & Sivapalan,  
509 1999; Troch et al., 2013; Vannier et al., 2014).

510 Fundamentally, the limited range inferred for the hydraulic conductivity comes from  
511 the sensitivity of the partitioning process between overland flows and groundwater flows  
512 in the discharge data. The contribution of baseflow and seepage flows sustaining the river  
513 discharge, estimated on average at 75 %, is indeed consistent with previous first-order  
514 estimates of around 60 % (Mougin et al., 2008; Aquilina et al., 2012; Clément et al., 2003)  
515 as well as with statistical filter estimates of around 79 % (Gustard et al., 1992; Lyne &  
516 Hollick, 1979). The contribution of overland flows is directly controlled by the distribu-  
517 tion of saturation along the hillslope (Kosugi et al., 2008; Montgomery et al., 1997; Wil-  
518 son & Dietrich, 1987; S. P. Anderson et al., 1997), which is set by the water table po-  
519 sition relative to the surface. At first order, this position of the water table is controlled  
520 by the hydraulic conductivity and not by the drainable porosity. This is intuitively il-  
521 lustrated by the absence of dependence of the steady-state groundwater flow equation  
522 on the drainable porosity. The drainable porosity only intervenes as a second-order con-  
523 trol for the typical seasonal dynamics of the water table and the subsequent seasonal base-  
524 flow contributions to the streamflow (Figure S8). This effectively explains why the drain-  
525 able porosity range cannot be constrained by the discharge datasets alone (Guérin et al.,  
526 2019). It also explains why the overall model uncertainty is not strongly impacted by  
527 the uncertainty of the drainable porosity.

$k$ [m/s]	$T$ [m <sup>2</sup> /s]	$\phi_d$ [-]	$\phi_{tot}$ [-]	Depth [m]	N	Settings	Reference
$1.8 \cdot 10^{-5}$	$3.1 \cdot 10^{-4}$	<b>0.080</b>	<b>0.29</b>	<b>17</b>	<b>28</b>	<b>Guillec: shallow granites</b>	<b>This study</b>
$8.0 \cdot 10^{-6}$		0.080	0.60	20	12	Kerrien, Kerbernez: shallow granites	Martin et al. (2006)
$3.6 \cdot 10^{-5}$		0.050		30	10	Kerrien, Kerbernez: shallow granites	Legchenko et al. (2004)
$1.0 \cdot 10^{-5}$				10	2	Pleine Fougères: weathered schists	Clément et al. (2003)
$6.3 \cdot 10^{-6}$			0.45	20	10	Pleine Fougères: weathered schists and granites	Kolbe et al. (2016)
$2.6 \cdot 10^{-6}$			0.21	50	10	Pleine Fougères: fractured schists and granites	Kolbe et al. (2016)
$5.1 \cdot 10^{-6}$		0.030		6	7	Kervidy: weathered schists	Molenat (1999)
$2.2 \cdot 10^{-6}$					4	Pont Lagot: weathered schists	Grimaldi et al. (2009)
$1.0 \cdot 10^{-5}$		0.013			2	Kervidy: weathered schists	Conan et al. (2003)
	$1.3 \cdot 10^{-5}$				2	Kervidy: fractured schists	Conan et al. (2003)
	$2.2 \cdot 10^{-3}$	0.037			11	Ploëmeur: transmissive zone, schists and granites	Leray et al. (2012)
	$6.0 \cdot 10^{-4}$			$\leq 25$	12	Ploëmeur: shallow schists	Le Borgne et al. (2006)
	$2.2 \cdot 10^{-4}$			$\geq 25$	22	Ploëmeur: deep granites	Le Borgne et al. (2006)
	$2.9 \cdot 10^{-3}$				23	Ploëmeur: schists and granites	Le Borgne et al. (2006)
	$7.3 \cdot 10^{-5}$	0.035		15	4	St Brice: weathered schists	Roques et al. (2014)
	$4.4 \cdot 10^{-4}$			50	7	St Brice: fractured schists	Roques et al. (2014)

**Table 1.** Logarithmic averaged measured or modeled hydraulic properties in Brittany aquifers. For each site, independent estimates are provided as well as typical depth of investigation when available. N is the number of independent values leading to these estimations. For more details, see Text S7.

528 Drainable and total porosities can however be at least partially constrained by CFC  
529 data. The drainable porosity  $\phi_d$  must be between 0.6 % and 25 %, and the total poros-  
530 ity  $\phi_{tot}$  between 15 % and 47 % (Figure 4.B). Such ranges are consistent with previous  
531 studies from which the drainable porosity inferred from well pumping tests or geochem-  
532 ical characteristics has been found between 2 % and 10 % (Legchenko et al., 2004; Mar-  
533 tin et al., 2006; Molenat, 1999; Leray et al., 2012; Roques et al., 2014) and the total poros-  
534 ity inferred with CFC data between 25 % and 45 % (Kolbe et al., 2016) (see Table 1).  
535 With these values, the porosities of the Guillec catchment would be further constrained

536 between 3 % and 12 % for  $\phi_d$  and between 20 and 30 % for  $\phi_{tot}$  (see purple rectangle  
537 on Figure 4.B). The range of  $\phi_{tot}$  might be quite high if not considering that the total  
538 porosity is a lumped way to represent the different processes and structures that delay  
539 the transport of solutes (Haggerty & Gorelick, 1995; Carrera et al., 1998).

#### 540 **4.2 The seasonal water table intersection with the land surface drives** 541 **the dynamics of the mean transit time $mTT$**

542 The streamwater mean transit time  $mTT$  is equal to 13 years, almost twice as large  
543 as the 7 years estimated previously on similar sites based on renewal rates (Mougin et  
544 al., 2015). Even though it is controlled by the averaged size of the groundwater storage  
545 like in other similar sites (Kolbe et al., 2016; Haitjema, 1995; Chesnaux et al., 2005), the  
546 mean transit time differs from the renewal rate defined as the groundwater storage di-  
547 vided by the recharge (Danckwerts, 1953). Two of the assumptions underlying the re-  
548 newal rate approximation noted in Harman (2014) and Berghuijs and Kirchner (2017)  
549 are not fulfilled. First, the modeled processes are inherently transient. Differences be-  
550 tween the steady state (i.e. obtained when the state variable  $S$  does not vary) and the  
551 stationary state (i.e. the average of the seasonal variations)  $mTT$  and  $mTT_{gw}$  are sig-  
552 nificant (Table S2). This is also clearly illustrated on Figure 7, where the steady state  
553 mean transit time of the groundwater contributions to the stream  $mTT_{gw}$  is significantly  
554 shorter than the seasonal  $mTT_{gw}$  variations. This comes from the non linearity of the  
555 model incorporating seepage areas that strongly depend on the precise water table lo-  
556 cation. Detailed explanations are given in Text S8. Second, the reservoir is not perfectly  
557 mixed. The transit time distribution is therefore rather power-law than exponential be-  
558 cause the reservoir remains stratified with only partial mixing and is limited at the wa-  
559 ter table by the seasonal intersection with the land surface.

560 These results confirm the measurements carried out regionally on several Brittany  
561 watersheds and more globally in temperate catchments (J. Yang et al., 2018). From a  
562 depth of a few meters below the water table, the residence time is greater than 10 years,  
563 but conversely, the yearly-flushed, variably saturated zone shows residence times on the  
564 order of one year (Ayraud et al., 2008; Legout et al., 2007; de Montety et al., 2018). The  
565 results obtained here make it possible to remove a contradiction between the observa-  
566 tions of residence times measured by tracers in groundwater which indicate long times  
567 and the fast processes generally associated with streamwater discharge dynamics. Long  
568 residence times in groundwater (through baseflow) together with a rapid component of  
569 transfer into the rivers (through overland and seepage flow) are not incompatible, rather  
570 they are linked through the seasonal water table fluctuations and groundwater strati-  
571 fication.

572 We further explore how these modeled processes control the temporal dynamics of  
573 the mean transit time  $mTT$ . To highlight their impact on the model results we perform  
574 two complementary simulations where we alternatively remove water table intersection  
575 and stratification from the reference model (squares in Figure 7). The reference model  
576 refers to the model, which has been used in this study (described in section 2). First,  
577 we removed the water table interactions with the land surface (stars in Figure 7) from  
578 the reference model by not considering the upper land surface boundary on the aquifer  
579 capacity (last equation of system of equations (1)). For this model, the seasonal dynam-  
580 ics of  $mTT$  almost vanishes with variations strongly limited to 1.7 years (Figure 7.A).

581 Second, we removed the groundwater stratification (diamonds in Figure 7) from the ref-  
 582 erence model. To do that, we relaxed the implicit condition stated in the second equa-  
 583 tion of system (3) that the particles exiting the first the aquifer at the seepage face are  
 584 the ones located at the top of the aquifer column. Instead, we developed an algorithm  
 585 that randomly samples particles, from any vertical location of a given numeric cell en-  
 586 counter seepage face. The right number of particles is retrieved to feed the seepage  
 587 flux by ensuring flux conservation. For this latter model, the seasonal dynamics of the  
 588 mean transit time is well preserved as well as its magnitude. The remaining differences  
 589 mainly occur during the dry season ( $\pm 4$  years at most during the September month) when  
 590 transit times are dominantly controlled by the proportion of groundwater contributions  
 591 to streamflow.

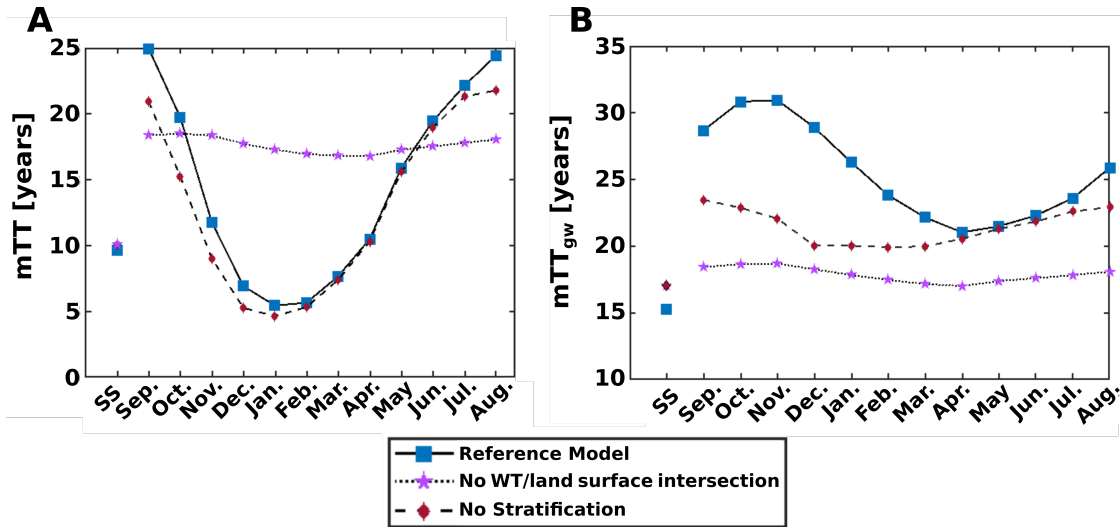


**Figure 7.** Investigation of the relative effects of the seasonal water table intersection with the land surface and of the groundwater flowpaths stratification for the steady state (SS) and interannual monthly averaged. Comparison of A. the mean transit time to the river  $mTT$  and B. the mean transit time of the groundwater contribution (baseflow and seepage flow) to the streamwater  $mTT_{gw}$  for the reference model (squares) and the models without intersection with the surface (stars) and without groundwater stratification (diamonds). The three models are parametrized with:  $k = 1.17 \cdot 10^{-5}$  m/s and  $\phi_d = \phi_{tot} = 24$  %. Note that the difference of vertical scales between the two figures.

592 Two compartments (here the surface and the aquifer), with different characteris-  
 593 tic transit times, are therefore needed to obtain seasonally varying  $mTT$ . Their dynam-  
 594 ical connection through water table intersection indeed generates temporary saturation  
 595 excess overland flow and seepage flow leading to seasonally varying  $mTT$ . With only the  
 596 groundwater compartment, the seasonally varying infiltration fluxes are dampened by  
 597 the groundwater storage volume and  $mTT$  becomes nearly constant. Groundwater strat-  
 598 ification alone has a notably smaller impact on the streamflow  $mTT$  since  $mTT$  vari-  
 599 ations are primarily controlled by the relative contribution of groundwater flows to the  
 600 stream and not by the internal organization of groundwater circulation inside the aquifer.

601 Here the short streamwater transit times come from the contribution of the sur-  
602 face compartment to the stream. While the groundwater compartment is key to explain  
603 the old transit times ( $\geq 1$  year old), faster flowpaths can be delivered by the surface or  
604 by the soil compartment. Deciphering the relative role of these shallower compartments  
605 would require other tracers than CFCs and a model running with finer timesteps (e.g.  
606 hourly to daily timesteps).

### 607 **4.3 Groundwater flowpath stratification is critical for the mean tran-** 608 **sit time of the groundwater contribution to the river $mTT_{gw}$**

609 While groundwater stratification is a second-order control of the mean transit time  
610 dynamics of the entire streamflow, it becomes essential for the mean transit time dynam-  
611 ics of the groundwater contribution to the river,  $mTT_{gw}$  (Figure 7.B). The simplified model  
612 without stratification (diamonds) misses the seasonal dynamics of the reference hillslope  
613 model (squares). Indeed, for the reference model,  $mTT_{gw}$  broadly varies by  $\pm 4$  years around  
614 a mean of 27 years. On the contrary, the model without groundwater stratification only  
615 varies by  $\pm 1.5$  years around a mean of 23 years. Randomly sampling the particles from  
616 the water column indeed removes the preference for the aquifer to release young water.  
617 On the contrary, the reference model, which respects the stratification of groundwater  
618 residence times, mostly samples young groundwater during the wet season, when such  
619 young particles are available at the top of the water column. During the dry season, only  
620 old groundwater particles remain to be sampled, reinforcing the seasonal variability of  
621  $mTT_{gw}$ .

622 The quantity  $mTT_{gw}$  is likely to be crucial when a precise representation of deep  
623 compartments is needed. This encompasses a broad range of topics, from studies assess-  
624 ing the impact of global climate change on transit times and water quality to studies in-  
625 terested in legacy effects of these groundwater storages, including geochemical processes  
626 where the interaction of reaction kinetics and transit times can be important (White et  
627 al., 1983). Both measured and model-derived water ages have been shown to correlate  
628 with weathering-derived solute chemistry in streams (Benettin et al., 2015; Rademacher  
629 et al., 2005). Geochemical tracer data such as Ge/Si ratios and stable isotopes of Si and  
630 Ca indicate that not only the flux but also the sources of solutes vary with discharge in  
631 studied streams (Kurtz et al., 2011; Cenko-Tok et al., 2009). The mechanism can include  
632 interactions with different materials along different flowpaths, but also differences in the  
633 time available for reaction progress as in kinetically limited systems (Fernandez et al.,  
634 2021). Integrated hydro-biogeochemical models, like the approach outlined here, rely-  
635 ing on partitioning flow and timing transport are therefore needed to address these hy-  
636 potheses.

### 637 **4.4 Limitations and perspectives**

638 While this parsimonious strategy effectively constrains the transit times of the ground-  
639 water circulation, some limitations arise from the conceptual representation of the sur-  
640 face and unsaturated zone processes. First, surface runoff processes are represented through  
641 a gravity-driven routing representation. This routing scheme neglects pre-event water  
642 present in the soil matrix, which can contribute to the flow. The presence of pre-event  
643 water could delay the estimated transit times of overland flowpaths by some months but  
644 will not significantly change the estimate of the mean transit times and the old compo-

645 nent of the streamwater transit times distributions. However, this limitation prevents  
646 us from applying the model in its current configuration at the daily to hourly timescale.  
647 Indeed, we would strongly underestimate runoff routing transit times that have been shown  
648 to be mainly made up of pre-event water (von Freyberg et al., 2018). Adding a more de-  
649 tailed runoff component but still parsimonious to this equivalent hillslope representation  
650 could be achieved through a total soil water storage description that could be partially  
651 mixed with the runoff routing. This would also enable the model to distinguish between  
652 the fast flowpaths arising at the surface or in the soil compartment (Heidbüchel et al.,  
653 2020). Second, this routing scheme process neglects re-infiltration typically occurring be-  
654 fore surface overland flow reaches the stream (Jackson et al., 2014; Klaus & Jackson, 2018;  
655 Gabrielli & McDonnell, 2020). In our model, most of the saturation excess overland flow  
656 is generated in the vicinity of the river. This proximity to the river might prevent re-  
657 infiltration (Jackson et al., 2014). Nevertheless, if re-infiltration occurs here, increased  
658 transit times would be less than one year as the groundwater transit times for water in-  
659 filtrating in the vicinity of the river is less than one year (Figure S10).

660 Another limitation refers to the transfers in the unsaturated zone, which have been  
661 neglected. Studies of transit times in the unsaturated zone in crystalline basement have  
662 shown that they are short (ca. 2 years) (Legout et al., 2007; de Montety et al., 2018),  
663 and so integration of an explicit representation of unsaturated zone transfer should have  
664 marginal impact on the longer transit times associated with groundwater flow. Indeed,  
665 in crystalline basements located in temperate climate, the unsaturated zone is quite shal-  
666 low (typically less than 5 meters, (Le Borgne et al., 2006; Roques et al., 2014; Marçais  
667 et al., 2018)). This could be different for other settings (arid climate, sedimentary set-  
668 tings), where the representation of percolation in the unsaturated zone will be a signif-  
669 icant part of the total transit times to the stream (Schwientek et al., 2009; Green et al.,  
670 2018; Chen et al., 2019). Adding a flux and transport representation of the vadose zone  
671 could be done with a 1D vertical model, which would preserve the parsimonious philoso-  
672 phy of the approach presented here for the saturated compartment (Harman et al., 2011).

673 All these limitations would increase the young transit times, but would have only  
674 small effects on the old transit times. Further, constraining these fast processes would  
675 require the addition of specific tracers well-suited for short transit times. Indeed, CFCs  
676 tracers cannot track transport in the unsaturated zone and are not adapted to the timescales  
677 below one year, which require intensive monitoring of stable water isotopes ( $^2H$ ,  $\delta^{18}O$ )  
678 or conservative solutes (chloride) (Sprenger et al., 2019; Harman, 2014; Benettin, Soulsby,  
679 et al., 2017).

680 An additional limitation in this study is related to the number of CFCs samples  
681 used to calibrate the model. We only relied on one sampling campaign on three differ-  
682 ent sampling sites to date the groundwater and its contribution to the river. A solution  
683 would be to sample more sites, e.g. by systematically sampling springs (Rademacher et  
684 al., 2001, 2005) or to sample CFCs at different seasons (Guillaumot et al., 2021). More  
685 intensive sampling indeed enables to link discharge (Morgenstern et al., 2010) or dissolved  
686 solutes concentrations to groundwater ages (Marçais et al., 2018), which offers oppor-  
687 tunities to strengthen the spatial and temporal resolution of transit times in the river  
688 (Peters et al., 2014).

## 5 Conclusion

Using a parsimonious approach that emphasizes 1) variable contributions from shallow and deep flow paths and 2) stratification of groundwater residence times, we have demonstrated how the groundwater contribution to streams control streamwater mean transit times and its seasonal variations in a crystalline bedrock catchment under temperate climate. The 2D model requires the calibration of the hydraulic conductivity, drainable porosity and total porosity from discharge time series and CFC data. In the catchment studied, all the calibrated models display significant groundwater contribution to stream (ca.  $75\pm 14\%$ ) with an average age of 17 years, leading to mean streamwater transit times on average equal to 13 years. All calibrated models display strong seasonal interactions between the water table and the land surface leading to a dynamic partitioning between groundwater flows (baseflow + seepage flow) and overland flows. This partitioning strongly conditions the seasonal dynamics of the streamwater mean transit times, from 6 years at high flow to 20 years at low flow.

The influence of the groundwater residence time stratification plays only a second-order role for the seasonal evolution of streamwater mean transit times, but is significant for the seasonal evolution of the mean transit times of the groundwater contribution to the stream. This last finding is likely to play a pivotal role for compounds which are predominantly found or generated in the aquifer. These may include solutes released from bedrock weathering or contaminants transported in groundwater.

The hillslope models show how (1) surface vs groundwater flow partitioning and (2) groundwater residence time stratification shape the transit time distributions. The understanding obtained through this study is particularly important for issues related to diffuse pollutant transfers and more generally to element transfers and biogeochemical fluxes within catchments. It is common for workers in the field to focus on in-stream processes and rapid dynamics that impact river flow, such as overland flow. Here we show that most of the streamwater has in fact resided underground for time scales of a decade or more and is delivered to the stream as baseflow and seepage flow. The decomposition of the flow sources also shows how the transfer of elements via groundwater is distributed between a fast component (one year for the seepage flow) and a much slower component (several tens of years for the baseflow), which indicates that changes in agricultural practices or land use will both have a rapid impact (ca. 1 year) and will also have impacts over the long term (tens of years). This complexity should be accounted for in watershed management.

## Acknowledgments

We acknowledge the Agence Nationale de la Recherche (ANR) for its funding through the "Investissements d'avenir" program under the project CZTOP (n°ANR-17-MPGA-0009). The model hs1D is available on github [github.com/jmarcais/hs1D\\_beta](https://github.com/jmarcais/hs1D_beta) (Marçais, 2021). Data used for this study are available at [doi.org/10.15454/UYX0EB](https://doi.org/10.15454/UYX0EB). We thank Aurélie Guillou, Virginie Vergnaud and Thierry Labasque for the chemical analysis in the Condote-Eau (Rennes 1) analytical platform and the help on the field. We thank Ciaran Harman for insightful discussions and Sylvain Kuppel for reviewing a former version of this manuscript.

## 732 Appendix A Separation of lateral and vertical velocity term

733 Considering that the water is incompressible, we have the relation  $\nabla \mathbf{v} = \frac{dv_x}{dx} +$   
 734  $\frac{dv_y}{dy} + \frac{dv_z}{dz} = 0$  (Strack, 1984; Pollock, 1988; Harman, 2019). Deriving  $v_x$  with respect  
 735 to  $x$  (cf. equation 2), we get:

$$736 \frac{dv_x}{dx} = \frac{\phi_d}{\phi_{tot}} v_x \left( \frac{1}{Q} \frac{dQ}{dx} - \frac{1}{S} \frac{dS}{dx} \right) \quad (7)$$

$$= \frac{\phi_d}{\phi_{tot}} v_x \left( \frac{1}{Q} \frac{dQ}{dx} - \frac{1}{h} \frac{dh}{dx} - \frac{1}{\omega} \frac{d\omega}{dx} \right)$$

737 Applying symmetry principles (Curie, 1894), we can attribute the part of this quan-  
 738 tity invariant to  $z$  to the quantity  $\frac{dv_y}{dy}$ :

$$739 \frac{dv_y}{dy} = \frac{\phi_d}{\phi_{tot}} \frac{1}{\omega} \frac{d\omega}{dx} v_x \quad (8)$$

740 This enables derivation of  $v_z$ :

$$741 \frac{dv_z}{dz} = -\frac{dv_x}{dx} - \frac{dv_y}{dy} \quad (9)$$

$$= -\frac{\phi_d}{\phi_{tot}} \left( \frac{d}{dx} \left( \frac{Q}{S} \right) + \frac{1}{\omega} \frac{d\omega}{dx} \frac{Q}{S} \right)$$

742 Hence, as  $\frac{dv_z}{dz}$  does not depend on  $z$ :

$$743 v_z = z \frac{dv_z}{dz} = -z \frac{\phi_d}{\phi_{tot}} \left( \frac{d}{dx} \left( \frac{Q}{S} \right) + \frac{1}{\omega} \frac{d\omega}{dx} \frac{Q}{S} \right) \quad (10)$$

744 2D flow lines  $\mathbf{x}(t) = (x(t), z(t))$  derive from the Lagrangian definition of velocity where  
 745 the temporal derivative of the trajectory  $\mathbf{x}(t)$  is linked to the velocity field:  $\frac{d\mathbf{x}}{dt} = \mathbf{v}(\mathbf{x}(t)) =$   
 746  $(v_x(x(t), z(t), t), v_z(x(t), z(t), t))$ .

## 747 References

- 748 Ameli, A. A., Beven, K., Erlandsson, M., Creed, I. F., McDonnell, J. J., & Bishop,  
 749 K. (2017). Primary weathering rates, water transit times, and concentration-  
 750 discharge relations: A theoretical analysis for the critical zone. *Water Resour.*  
 751 *Res.*, *53*(1), 942–960. doi: 10.1002/2016WR019448
- 752 Anderson, R. S., Rajaram, H., & Anderson, S. P. (2019). Climate driven coevo-  
 753 lution of weathering profiles and hillslope topography generates dramatic  
 754 differences in critical zone architecture. *Hydrol. Process.*, *33*(1), 4–19. doi:  
 755 10.1002/hyp.13307
- 756 Anderson, S. P., Dietrich, W. E., Montgomery, D. R., Torres, R., Conrad, M. E., &  
 757 Loague, K. (1997). Subsurface flow paths in a steep, unchanneled catchment.  
 758 *Water Resour. Res.*, *33*(12), 2637–2653. doi: 10.1029/97WR02595
- 759 Aquilina, L., Vergnaud-Ayraud, V., Labasque, T., Bour, O., Molénat, J., Ruiz, L.,  
 760 ... Longuevergne, L. (2012). Nitrate dynamics in agricultural catchments  
 761 deduced from groundwater dating and long-term nitrate monitoring in surface-

- 762 and groundwaters. *Science of The Total Environment*, 435–436, 167–178. doi:  
763 10.1016/j.scitotenv.2012.06.028
- 764 Ayraud, V., Aquilina, L., Labasque, T., Pauwels, H., Molenat, J., Pierson-  
765 Wickmann, A.-C., ... Davy, P. (2008). Compartmentalization of physical  
766 and chemical properties in hard-rock aquifers deduced from chemical and  
767 groundwater age analyses. *Applied Geochemistry*, 23(9), 2686–2707. doi:  
768 10.1016/j.apgeochem.2008.06.001
- 769 Benettin, P., Bailey, S. W., Rinaldo, A., Likens, G. E., McGuire, K. J., & Botter, G.  
770 (2017). Young runoff fractions control streamwater age and solute concentra-  
771 tion dynamics. *Hydrol. Process.*, 31(16), 2982–2986. doi: 10.1002/hyp.11243
- 772 Benettin, P., & Bertuzzo, E. (2018). Tran-SAS v1.0: A numerical model to com-  
773 pute catchment-scale hydrologic transport using StorAge Selection functions.  
774 *Geosci. Model Dev.*, 11(4), 1627–1639. doi: 10.5194/gmd-11-1627-2018
- 775 Benettin, P., Scott W. Bailey, Campbell, J. L., Green, M., Rinaldo, A., Likens Gene  
776 E., ... Botter Gianluca (2015). Linking water age and solute dynamics in  
777 streamflow at the Hubbard Brook Experimental Forest, NH, USA. *Water*  
778 *Resources Research*, 51(11), 9256–9272. doi: 10.1002/2015WR017552
- 779 Benettin, P., Soulsby, C., Birkel, C., Tetzlaff, D., Botter, G., & Rinaldo, A. (2017).  
780 Using SAS functions and high-resolution isotope data to unravel travel time  
781 distributions in headwater catchments. *Water Resour. Res.*, 53(3), 1864–1878.  
782 doi: 10.1002/2016WR020117
- 783 Berghuijs, W. R., & Kirchner, J. W. (2017). The relationship between contrast-  
784 ing ages of groundwater and streamflow: Connecting Storage and Streamflow  
785 Ages. *Geophys. Res. Lett.*, 44(17), 8925–8935. doi: 10.1002/2017GL074962
- 786 Blume, T., & van Meerveld, H. I. (2015). From hillslope to stream: Methods to  
787 investigate subsurface connectivity: Methods to investigate subsurface connec-  
788 tivity. *WIREs Water*, 2(3), 177–198. doi: 10.1002/wat2.1071
- 789 Boone, A., Samuelsson, P., Gollvik, S., Napoly, A., Jarlan, L., Brun, E., &  
790 Decharme, B. (2017). The interactions between soil–biosphere–atmosphere  
791 land surface model with a multi-energy balance (ISBA-MEB) option in SUR-  
792 FEXv8 – Part 1: Model description. *Geosci. Model Dev.*, 10(2), 843–872. doi:  
793 10.5194/gmd-10-843-2017
- 794 Botter, M., Li, L., Hartmann, J., Burlando, P., & Fatichi, S. (2020). Depth of Solute  
795 Generation Is a Dominant Control on Concentration-Discharge Relations. *Wa-  
796 ter Resour. Res.*, 56(8), e2019WR026695. doi: 10.1029/2019WR026695
- 797 Boussinesq, J. (1877). *Essai sur la théorie des eaux courantes*. Imprimerie Na-  
798 tionale.
- 799 Brantley, S. L., McDowell, W. H., Dietrich, W. E., White, T. S., Kumar, P., An-  
800 derson, S. P., ... Gaillardet, J. (2017). Designing a network of critical zone  
801 observatories to explore the living skin of the terrestrial Earth. *Earth Surf.  
802 Dyn.*, 5(4), 841–860. doi: 10.5194/esurf-5-841-2017
- 803 Brutsaert, W. B., & Nieber, J. L. (1977). Regionalized drought flow hydrographs  
804 from a mature glaciated plateau. *Water Resour. Res.*, 13(3), 637–643. doi: 10  
805 .1029/WR013i003p00637
- 806 Camporese, M., Paniconi, C., Putti, M., & Orlandini, S. (2010). Surface-subsurface  
807 flow modeling with path-based runoff routing, boundary condition-based cou-  
808 pling, and assimilation of multisource observation data. *Water Resour. Res.*,  
809 46(2), W02512. doi: 10.1029/2008WR007536

- 810 Carrera, J., Sánchez-Vila, X., Benet, I., Medina, A., Galarza, G., & Guimerà, J.  
811 (1998). On matrix diffusion: Formulations, solution methods and qualitative  
812 effects. *Hydrogeology Journal*, 6(1), 178–190. doi: 10.1007/s100400050143
- 813 Cenki-Tok, B., Chabaux, F., Lemarchand, D., Schmitt, A. D., Pierret, M. C.,  
814 Viville, D., ... Stille, P. (2009). The impact of water–rock interaction and  
815 vegetation on calcium isotope fractionation in soil- and stream waters of a  
816 small, forested catchment (the Strengbach case). *Geochimica et Cosmochimica*  
817 *Acta*, 73(8), 2215–2228. doi: 10.1016/j.gca.2009.01.023
- 818 Chen, N., Valdes, D., Marlin, C., Blanchoud, H., Guerin, R., Rouelle, M., & Rib-  
819 stein, P. (2019). Water, nitrate and atrazine transfer through the unsaturated  
820 zone of the Chalk aquifer in northern France. *Science of The Total Environ-*  
821 *ment*, 652, 927–938. doi: 10.1016/j.scitotenv.2018.10.286
- 822 Chesnaux, R., Molson, J., & Chapuis, R. (2005). An Analytical Solution for Ground  
823 Water Transit Time through Unconfined Aquifers. *Ground Water*, 43(4), 511–  
824 517. doi: 10.1111/j.1745-6584.2005.0056.x
- 825 Clément, J.-C., Holmes, R. M., Peterson, B. J., & Pinay, G. (2003). Isotopic inves-  
826 tigation of denitrification in a riparian ecosystem in western France. *J. Appl.*  
827 *Ecol.*, 40(6), 1035–1048. Retrieved from [http://onlinelibrary.wiley.com/](http://onlinelibrary.wiley.com/doi/10.1111/j.1365-2664.2003.00854.x/full)  
828 [doi/10.1111/j.1365-2664.2003.00854.x/full](http://onlinelibrary.wiley.com/doi/10.1111/j.1365-2664.2003.00854.x/full)
- 829 Conan, C., Bouraoui, F., Turpin, N., de Marsily, G., & Bidoglio, G. (2003). Mod-  
830 eling Flow and Nitrate Fate at Catchment Scale in Brittany (France). *J. Envi-*  
831 *ron. Qual.*, 32(6), 2026–2032. doi: 10.2134/jeq2003.2026
- 832 Curie, P. (1894). Sur la symétrie dans les phénomènes physiques, symétrie d’un  
833 champ électrique et d’un champ magnétique. *J. Phys. Theor. Appl.*, 3(1), 393–  
834 415. doi: 10.1051/jphystap:018940030039300
- 835 Danckwerts, P. V. (1953). Continuous flow systems: Distribution of residence times.  
836 *Chemical Engineering Science*, 2(1), 1–13. doi: 10.1016/0009-2509(53)80001  
837 -1
- 838 de Dreuzy, J.-R., Beaudoin, A., & Erhel, J. (2007). Asymptotic dispersion in 2D het-  
839 erogeneous porous media determined by parallel numerical simulations. *Water*  
840 *Resour. Res.*, 43(10). doi: 10.1029/2006WR005394
- 841 de Dreuzy, J.-R., Carrera, J., Dentz, M., & Borgne, T. L. (2012). Asymp-  
842 totic dispersion for two-dimensional highly heterogeneous permeability  
843 fields under temporally fluctuating flow. *Water Resour. Res.*, 48(1). doi:  
844 10.1029/2011WR011129
- 845 Dunkle, S. A., Plummer, L. N., Busenberg, E., Phillips, P. J., Denver, J. M., Hamil-  
846 ton, P. A., ... Coplen, T. B. (1993). Chlorofluorocarbons (CCl<sub>3</sub>F and  
847 CCl<sub>2</sub>F<sub>2</sub>) as dating tools and hydrologic tracers in shallow groundwater of  
848 the Delmarva Peninsula, Atlantic Coastal Plain, United States. *Water Resour.*  
849 *Res.*, 29(12), 3837–3860. doi: 10.1029/93WR02073
- 850 Dupuit, J. (1863). *Études théoriques et pratiques sur le mouvement des eaux*  
851 *dans les canaux découverts et à travers les terrains perméables : avec des*  
852 *considérations relatives au régime des grandes eaux, au débouché à leur don-*  
853 *ner, et à la marche des alluvions dans les rivières à fond mobile (2e édition*  
854 *revue et considérablement augmentée) / par J. Dupuit...* Retrieved from  
855 <https://gallica.bnf.fr/ark:/12148/bpt6k62096061>
- 856 Ehrhardt, S., Kumar, R., Fleckenstein, J. H., Attinger, S., & Musolff, A. (2019).  
857 Trajectories of nitrate input and output in three nested catchments along

- 858 a land use gradient. *Hydrol. Earth Syst. Sci.*, *23*(9), 3503–3524. doi:  
 859 10.5194/hess-23-3503-2019
- 860 Engdahl, N. B., & Maxwell, R. M. (2014). Approximating groundwater age distribu-  
 861 tions using simple streamtube models and multiple tracers. *Advances in Water*  
 862 *Resources*, *66*, 19–31. doi: 10.1016/j.advwatres.2014.02.001
- 863 Engesgaard, P., Højberg, A. L., Hinsby, K., Jensen, K. H., Laier, T., Larsen, F.,  
 864 ... Plummer, L. N. (2004). Transport and Time Lag of Chlorofluorocarbon  
 865 Gases in the Unsaturated Zone, Rabis Creek, Denmark. *Vadose Zone J.*, *3*(4),  
 866 1249–1261. doi: 10.2136/vzj2004.1249
- 867 Fan, Y., & Bras, R. L. (1998). Analytical solutions to hillslope subsurface storm  
 868 flow and saturation overland flow. *Water Resour. Res.*, *34*(4), 921–927. doi: 10  
 869 .1029/97WR03516
- 870 Fang, Z., Carroll, R. W. H., Schumer, R., Harman, C., Wilusz, D., & Williams,  
 871 K. H. (2019). Streamflow partitioning and transit time distribution in snow-  
 872 dominated basins as a function of climate. *Journal of Hydrology*, *570*, 726–738.  
 873 doi: 10.1016/j.jhydrol.2019.01.029
- 874 Farr, T. G., Rosen, P. A., Caro, E., Crippen, R., Duren, R., Hensley, S., ... Alsdorf,  
 875 D. (2007). The Shuttle Radar Topography Mission. *Rev. Geophys.*, *45*(2),  
 876 RG2004. doi: 10.1029/2005RG000183
- 877 Fatchi, S., Vivoni, E. R., Ogden, F. L., Ivanov, V. Y., Mirus, B., Gochis, D., ...  
 878 Tarboton, D. (2016). An overview of current applications, challenges, and  
 879 future trends in distributed process-based models in hydrology. *Journal of*  
 880 *Hydrology*, *537*, 45–60. doi: 10.1016/j.jhydrol.2016.03.026
- 881 Ferguson, G., Cuthbert, M., Befus, K. M., Gleeson, T., & McIntosh, J. C. (2020).  
 882 *The groundwater age-sustainability myth* (Preprint). EarthArXiv. doi:  
 883 10.31223/osf.io/gq2m3
- 884 Fernandez, N. M., Perez-Fodich, A., Derry, L. A., & Druhan, J. L. (2021). A first  
 885 look at Ge/Si partitioning during amorphous silica precipitation: Implications  
 886 for Ge/Si as a tracer of fluid-silicate interactions. *Geochimica et Cosmochimica*  
 887 *Acta*, *297*, 158–178. doi: 10.1016/j.gca.2021.01.007
- 888 Freer, J., McDonnell, J. J., Beven, K. J., Peters, N. E., Burns, D. A., Hooper, R. P.,  
 889 ... Kendall, C. (2002). The role of bedrock topography on subsurface storm  
 890 flow. *Water Resour. Res.*, *38*(12), 1269. doi: 10.1029/2001WR000872
- 891 von Freyberg, J., Studer, B., Rinderer, M., & Kirchner, J. W. (2018). Studying  
 892 catchment storm response using event and pre-event water volumes as frac-  
 893 tions of precipitation rather than discharge. *Hydrol. Earth Syst. Sci. Discuss.*,  
 894 1–34. doi: 10.5194/hess-2018-401
- 895 Frisbee, M. D., Wilson, J. L., Gomez-Velez, J. D., Phillips, F. M., & Campbell,  
 896 A. R. (2013). Are we missing the tail (and the tale) of residence time dis-  
 897 tributions in watersheds? *Geophys. Res. Lett.*, *40*(17), 4633–4637. doi:  
 898 10.1002/grl.50895
- 899 Gabrielli, C. P., & McDonnell, J. J. (2020). Modifying the Jackson index to quan-  
 900 tify the relationship between geology, landscape structure, and water tran-  
 901 sit time in steep wet headwaters. *Hydrol. Process.*, *34*(9), 2139–2150. doi:  
 902 10.1002/hyp.13700
- 903 Gabrielli, C. P., Morgenstern, U., Stewart, M. K., & McDonnell, J. J. (2018). Con-  
 904 trasting Groundwater and Streamflow Ages at the Maimai Watershed. *Water*  
 905 *Resour. Res.*, *54*(6), 3937–3957. doi: 10.1029/2017WR021825

- 906 Gardner, W. P., Harrington, G. A., Solomon, D. K., & Cook, P. G. (2011). Using  
 907 terrigenic  $^4\text{He}$  to identify and quantify regional groundwater discharge to  
 908 streams. *Water Resour. Res.*, *47*(6). doi: 10.1029/2010WR010276
- 909 Gauvain, A., Leray, S., Marçais, J., Roques, C., Vautier, C., Gresselin, F., ... de  
 910 Dreuzy, J.-R. (2021). Geomorphological Controls on Groundwater Transit  
 911 Times: A Synthetic Analysis at the Hillslope Scale. *Water Resour. Res.*, *57*(7),  
 912 e2020WR029463. doi: 10.1029/2020WR029463
- 913 Gelhar, L. W., & Axness, C. L. (1983). Three-dimensional stochastic analysis of  
 914 macrodispersion in aquifers. *Water Resour. Res.*, *19*(1), 161–180. doi: 10.1029/  
 915 WR019i001p00161
- 916 Gelhar, L. W., Welty, C., & Rehfeldt, K. R. (1992). A critical review of data on  
 917 field-scale dispersion in aquifers. *Water Resour. Res.*, *28*(7), 1955–1974. doi:  
 918 10.1029/92WR00607
- 919 Gleeson, T., & Manning, A. H. (2008). Regional groundwater flow in mountain-  
 920 ous terrain: Three-dimensional simulations of topographic and hydrogeologic  
 921 controls. *Water Resour. Res.*, *44*(10). doi: 10.1029/2008WR006848
- 922 Green, C. T., Liao, L., Nolan, B. T., Juckem, P. F., Shope, C. L., Tesoriero, A. J.,  
 923 & Jurgens, B. C. (2018). Regional Variability of Nitrate Fluxes in the Unsat-  
 924 urated Zone and Groundwater, Wisconsin, USA. *Water Resour. Res.*, *54*(1),  
 925 301–322. doi: 10.1002/2017WR022012
- 926 Grimaldi, C., Thomas, Z., Fossey, M., Fauvel, Y., & Merot, P. (2009). High chloride  
 927 concentrations in the soil and groundwater under an oak hedge in the West  
 928 of France: An indicator of evapotranspiration and water movement. *Hydrol.*  
 929 *Process.*, *23*(13), 1865–1873. doi: 10.1002/hyp.7316
- 930 Guérin, A., Devauchelle, O., Robert, V., Kitou, T., Dessert, C., Quiquerez, A., ...  
 931 Lajeunesse, E. (2019). Stream-Discharge Surges Generated by Groundwater  
 932 Flow. *Geophys. Res. Lett.*, *46*(13), 7447–7455. doi: 10.1029/2019GL082291
- 933 Guillaumot, L., Marçais, J., Vautier, C., Guillou, A., Vergnaud, V., Bouchez, C., ...  
 934 Aquilina, L. (2021). A hillslope-scale aquifer-model to determine past agricul-  
 935 tural legacy and future nitrate concentrations in rivers. *Science of The Total*  
 936 *Environment*, 149216. doi: 10.1016/j.scitotenv.2021.149216
- 937 Gupta, H. V., Kling, H., Yilmaz, K. K., & Martinez, G. F. (2009). Decomposition  
 938 of the mean squared error and NSE performance criteria: Implications for im-  
 939 proving hydrological modelling. *Journal of Hydrology*, *377*(1), 80–91. doi:  
 940 10.1016/j.jhydrol.2009.08.003
- 941 Gustard, A., Bullock, A., & Dixon, J. M. (1992). *Low flow estimation in the United*  
 942 *Kingdom*. Institute of Hydrology.
- 943 Haggerty, R., & Gorelick, S. M. (1995). Multiple-Rate Mass Transfer for Modeling  
 944 Diffusion and Surface Reactions in Media with Pore-Scale Heterogeneity. *Wa-*  
 945 *ter Resour. Res.*, *31*(10), 2383–2400. doi: 10.1029/95WR10583
- 946 Haitjema, H. M. (1995). On the residence time distribution in idealized groundwa-  
 947 tersheds. *Journal of Hydrology*, *172*(1), 127–146. doi: 10.1016/0022-1694(95)  
 948 02732-5
- 949 Haitjema, H. M., & Mitchell-Bruker, S. (2005). Are Water Tables a Subdued Replica  
 950 of the Topography? *Groundwater*, *43*(6), 781–786. doi: 10.1111/j.1745-6584  
 951 .2005.00090.x
- 952 Harman, C. J. (2014). Time-variable transit time distributions and transport: The-  
 953 ory and application to storage-dependent transport of chloride in a watershed.

- 954 *Water Resources Research*, 51(1), 1–30. doi: 10.1002/2014WR015707
- 955 Harman, C. J. (2019). Age-Ranked Storage-Discharge Relations: A Unified Descrip-  
 956 tion of Spatially Lumped Flow and Water Age in Hydrologic Systems. *Water*  
 957 *Resour. Res.*, 55(8), 7143–7165. doi: 10.1029/2017WR022304
- 958 Harman, C. J., Rao, P. S. C., Basu, N. B., McGrath, G. S., Kumar, P., & Siva-  
 959 palan, M. (2011). Climate, soil, and vegetation controls on the tempo-  
 960 ral variability of vadose zone transport. *Water Resour. Res.*, 47(10). doi:  
 961 10.1029/2010WR010194
- 962 Heimbüchel, I., Troch, P. A., & Lyon, S. W. (2013). Separating physical and meteo-  
 963 rological controls of variable transit times in zero-order catchments. *Water Re-*  
 964 *sour. Res.*, 49(11), 7644–7657. doi: 10.1002/2012WR013149
- 965 Heimbüchel, I., Troch, P. A., Lyon, S. W., & Weiler, M. (2012). The master transit  
 966 time distribution of variable flow systems. *Water Resour. Res.*, 48(6), W06520.  
 967 doi: 10.1029/2011WR011293
- 968 Heimbüchel, I., Yang, J., Musolff, A., Troch, P., Ferré, T., & Fleckenstein, J. H.  
 969 (2020). On the shape of forward transit time distributions in low-order  
 970 catchments. *Hydrol. Earth Syst. Sci.*, 24(6), 2895–2920. doi: 10.5194/  
 971 hess-24-2895-2020
- 972 Hunt, B. (1998). Contaminant Source Solutions with Scale-Dependent Dispersivi-  
 973 ties. *Journal of Hydrologic Engineering*, 3(4), 268–275. doi: 10.1061/(ASCE)  
 974 1084-0699(1998)3:4(268)
- 975 Jackson, C. R., Bitew, M., & Du, E. (2014). When interflow also percolates: Downs-  
 976 slope travel distances and hillslope process zones. *Hydrol. Process.*, 28(7), 3195–  
 977 3200. doi: 10.1002/hyp.10158
- 978 Jasechko, S., Kirchner, J. W., Welker, J. M., & McDonnell, J. J. (2016). Substantial  
 979 proportion of global streamflow less than three months old. *Nat. Geosci.*, 9(2),  
 980 126–129. doi: 10.1038/ngeo2636
- 981 Kaandorp, V. P., Louw, P. G. B., Velde, Y., & Broers, H. P. (2018). Transient  
 982 Groundwater Travel Time Distributions and Age-Ranked Storage-Discharge  
 983 Relationships of Three Lowland Catchments. *Water Resour. Res.*, 54(7),  
 984 4519–4536. doi: 10.1029/2017WR022461
- 985 Kazemi, G. A., Lehr, J. H., & Perrochet, P. (2006). *Groundwater Age*. John Wiley &  
 986 Sons.
- 987 Kirchner, J. W. (2016). Aggregation in environmental systems - Part 1: Seasonal  
 988 tracer cycles quantify young water fractions, but not mean transit times, in  
 989 spatially heterogeneous catchments. *Hydrol. Earth Syst. Sci.*, 20(1), 279–297.  
 990 doi: 10.5194/hess-20-279-2016
- 991 Kirchner, J. W., Feng, X., & Neal, C. (2000). Fractal stream chemistry and its  
 992 implications for contaminant transport in catchments. *Nature*, 403(6769), 524.  
 993 doi: 10.1038/35000537
- 994 Kirchner, J. W., Feng, X., & Neal, C. (2001). Catchment-scale advection and disper-  
 995 sion as a mechanism for fractal scaling in stream tracer concentrations. *Jour-*  
 996 *nal of Hydrology*, 254(1–4), 82–101. doi: 10.1016/S0022-1694(01)00487-5
- 997 Klaus, J., & Jackson, C. R. (2018). Interflow Is Not Binary: A Continuous Shallow  
 998 Perched Layer Does Not Imply Continuous Connectivity. *Water Resour. Res.*,  
 999 54(9), 5921–5932. doi: 10.1029/2018WR022920
- 1000 Kolbe, T., de Dreuzy, J.-R., Abbott, B. W., Aquilina, L., Babey, T., Green, C. T.,  
 1001 ... Pinay, G. (2019). Stratification of reactivity determines nitrate removal in

- 1002 groundwater. *PNAS*, 201816892. doi: 10.1073/pnas.1816892116
- 1003 Kolbe, T., Marçais, J., de Dreuzy, J.-R., Labasque, T., & Bishop, K. (2020). Lagged  
1004 rejuvenation of groundwater indicates internal flow structures and hydrological  
1005 connectivity. *Hydrol. Process.*, 34(10), 2176–2189. doi: 10.1002/hyp.13753
- 1006 Kolbe, T., Marçais, J., Thomas, Z., Abbott, B. W., de Dreuzy, J.-R., Rousseau-  
1007 Gueutin, P., ... Pinay, G. (2016). Coupling 3D groundwater modeling  
1008 with CFC-based age dating to classify local groundwater circulation in an  
1009 unconfined crystalline aquifer. *Journal of Hydrology*, 543, 31–46. doi:  
1010 10.1016/j.jhydrol.2016.05.020
- 1011 Kollet, S. J., & Maxwell, R. M. (2006). Integrated surface–groundwater flow mod-  
1012 eling: A free-surface overland flow boundary condition in a parallel ground-  
1013 water flow model. *Advances in Water Resources*, 29(7), 945–958. doi:  
1014 10.1016/j.advwatres.2005.08.006
- 1015 Kosugi, K., Katsura, S., Mizuyama, T., Okunaka, S., & Mizutani, T. (2008).  
1016 Anomalous behavior of soil mantle groundwater demonstrates the major ef-  
1017 fects of bedrock groundwater on surface hydrological processes. *Water Resour.*  
1018 *Res.*, 44(1). doi: 10.1029/2006WR005859
- 1019 Kuppel, S., Tetzlaff, D., Maneta, M. P., & Soulsby, C. (2020). Critical Zone Storage  
1020 Controls on the Water Ages of Ecohydrological Outputs. *Geophys. Res. Lett.*,  
1021 47(16), e2020GL088897. doi: 10.1029/2020GL088897
- 1022 Kurtz, A. C., Lugolobi, F., & Salvucci, G. (2011). Germanium-silicon as a flow path  
1023 tracer: Application to the Rio Icacos watershed. *Water Resources Research*,  
1024 47(6). doi: 10.1029/2010WR009853
- 1025 Labasque, T., Aquilina, L., Vergnaud, V., & Barbecot, F. (2014). Inter-laboratory  
1026 comparison of the analyses of sulphur hexafluoride (SF6) and three chlorofluo-  
1027 rocarbons (CFC-11, -12 and -113) in groundwater and an air standard. *Applied*  
1028 *Geochemistry*, 50, 118–129. doi: 10.1016/j.apgeochem.2014.03.009
- 1029 Le Borgne, T., Bour, O., Paillet, F. L., & Caudal, J. P. (2006). Assessment of pref-  
1030 erential flow path connectivity and hydraulic properties at single-borehole and  
1031 cross-borehole scales in a fractured aquifer. *Journal of Hydrology*, 328(1–2),  
1032 347–359. doi: 10.1016/j.jhydrol.2005.12.029
- 1033 Legchenko, A., Baltassat, J.-M., Bobachev, A., Martin, C., Robain, H., & Vouil-  
1034 lamoz, J.-M. (2004). Magnetic Resonance Sounding Applied to Aquifer  
1035 Characterization. *Groundwater*, 42(3), 363–373. doi: 10.1111/j.1745-6584.2004  
1036 .tb02684.x
- 1037 Legout, C., Molenat, J., Aquilina, L., Gascuel-Oudou, C., Faucheux, M., Fauvel, Y.,  
1038 & Bariac, T. (2007). Solute transfer in the unsaturated zone-groundwater  
1039 continuum of a headwater catchment. *Journal of Hydrology*, 332(3), 427–441.  
1040 doi: 10.1016/j.jhydrol.2006.07.017
- 1041 Le Moigne, P., Besson, F., Martin, E., Boé, J., Boone, A., Decharme, B., ...  
1042 Rousset-Regimbeau, F. (2020). The latest improvements with SURFEX  
1043 v8.0 of the Safran–Isba–Modcou hydrometeorological model for France. *Geosci.*  
1044 *Model Dev.*, 13(9), 3925–3946. doi: 10.5194/gmd-13-3925-2020
- 1045 Leray, S., de Dreuzy, J. R., Bour, O., Labasque, T., & Aquilina, L. (2012). Contri-  
1046 bution of age data to the characterization of complex aquifers. *Journal of Hy-*  
1047 *drology*, 464–465, 54–68. doi: 10.1016/j.jhydrol.2012.06.052
- 1048 Li, L., Maher, K., Navarre-Sitchler, A., Druhan, J., Meile, C., Lawrence, C.,  
1049 ... Beisman, J. (2017). Expanding the role of reactive transport mod-

- 1050 els in critical zone processes. *Earth-Science Reviews*, 165, 280–301. doi:  
 1051 10.1016/j.earscirev.2016.09.001
- 1052 Loritz, R., Hassler, S. K., Jackisch, C., Allroggen, N., van Schaik, L., Wien-  
 1053 höfer, J., & Zehe, E. (2017). Picturing and modeling catchments by rep-  
 1054 resentative hillslopes. *Hydrol. Earth Syst. Sci.*, 21(2), 1225–1249. doi:  
 1055 10.5194/hess-21-1225-2017
- 1056 L’vovich, M. I. (1979). *World Water Resources and Their Future*. Washington, D.  
 1057 C.: American Geophysical Union. doi: 10.1029/SP013
- 1058 Lyne, V., & Hollick, M. (1979). Stochastic time-variable rainfall-runoff modelling.  
 1059 In *Institute of Engineers Australia National Conference* (Vol. 1979, pp. 89–93).  
 1060 Institute of Engineers Australia Barton, Australia.
- 1061 Maher, K. (2010). The dependence of chemical weathering rates on fluid residence  
 1062 time. *Earth and Planetary Science Letters*, 294(1–2), 101–110. doi: 10.1016/  
 1063 j.epsl.2010.03.010
- 1064 Maher, K. (2011). The role of fluid residence time and topographic scales in deter-  
 1065 mining chemical fluxes from landscapes. *Earth and Planetary Science Letters*,  
 1066 312(1), 48–58. doi: 10.1016/j.epsl.2011.09.040
- 1067 Maher, K., & Druhan, J. (2014). Relationships between the Transit Time of Wa-  
 1068 ter and the Fluxes of Weathered Elements through the Critical Zone. *Procedia*  
 1069 *Earth and Planetary Science*, 10, 16–22. doi: 10.1016/j.proeps.2014.08.004
- 1070 Małoszewski, P., & Zuber, A. (1982). Determining the turnover time of groundwater  
 1071 systems with the aid of environmental tracers: 1. Models and their applicabil-  
 1072 ity. *Journal of Hydrology*, 57(3), 207–231. doi: 10.1016/0022-1694(82)90147-0
- 1073 Manning, A. H., Clark, J. F., Diaz, S. H., Rademacher, L. K., Earman, S., &  
 1074 Niel Plummer, L. (2012). Evolution of groundwater age in a mountain wa-  
 1075 tershed over a period of thirteen years. *Journal of Hydrology*, 460–461, 13–28.  
 1076 doi: 10.1016/j.jhydrol.2012.06.030
- 1077 Marçais, J. (2021). *Jmarçais/hs1D\_beta: hs1D flux and transport*. Zenodo. doi: 10  
 1078 .5281/zenodo.5234909
- 1079 Marçais, J., de Dreuzy, J. R., & Erhel, J. (2017). Dynamic coupling of sub-  
 1080 surface and seepage flows solved within a regularized partition formula-  
 1081 tion. *Advances in Water Resources*, 109(Supplement C), 94–105. doi:  
 1082 10.1016/j.advwatres.2017.09.008
- 1083 Marçais, J., de Dreuzy, J. R., Ginn, T. R., Rousseau-Gueutin, P., & Leray, S.  
 1084 (2015). Inferring transit time distributions from atmospheric tracer data:  
 1085 Assessment of the predictive capacities of Lumped Parameter Models on  
 1086 a 3D crystalline aquifer model. *Journal of Hydrology*, 525, 619–631. doi:  
 1087 10.1016/j.jhydrol.2015.03.055
- 1088 Marçais, J., Gauvain, A., Labasque, T., Abbott, B. W., Pinay, G., Aquilina, L., ...  
 1089 de Dreuzy, J.-R. (2018). Dating groundwater with dissolved silica and CFC  
 1090 concentrations in crystalline aquifers. *Science of The Total Environment*, 636,  
 1091 260–272. doi: 10.1016/j.scitotenv.2018.04.196
- 1092 de Marsily, G. (1986). *Quantitative hydrogeology: Groundwater hydrology for engi-  
 1093 neers*. Academic Press.
- 1094 Martin, C., Molénat, J., Gascuel-Oudou, C., Vouillamoz, J. M., Robain, H., Ruiz,  
 1095 L., ... Aquilina, L. (2006). Modelling the effect of physical and chem-  
 1096 ical characteristics of shallow aquifers on water and nitrate transport in  
 1097 small agricultural catchments. *Journal of Hydrology*, 326(1–4), 25–42. doi:

- 1098 10.1016/j.jhydrol.2005.10.040
- 1099 Maxwell, R. M., Condon, L. E., Kollet, S. J., Maher, K., Haggerty, R., & For-
- 1100 rester, M. M. (2016). The imprint of climate and geology on the resi-
- 1101 dence times of groundwater. *Geophys. Res. Lett.*, 2015GL066916. doi:
- 1102 10.1002/2015GL066916
- 1103 McDonnell, J. J. (2017). *Beyond the water balance* [Comments and Opinion]. doi: 10
- 1104 .1038/ngeo2964
- 1105 McDonnell, J. J., & Beven, K. (2014). Debates—The future of hydrological sciences:
- 1106 A (common) path forward? a call to action aimed at understanding velocities,
- 1107 celerities and residence time distributions of the headwater hydrograph. *Water*
- 1108 *Resour. Res.*, 50(6), 5342–5350. doi: 10.1002/2013WR015141
- 1109 Molenat, J. (1999). *Rôle de la nappe sur les transferts d'eau et de nitrate dans un*
- 1110 *bassin versant agricole : étude expérimentale et modélisation* (Doctoral disser-
- 1111 tation, Rennes 1). Retrieved from <http://www.theses.fr/1999REN1A004>
- 1112 de Montety, V., Aquilina, L., Labasque, T., Chatton, E., Fovet, O., Ruiz, L., ...
- 1113 de Dreuzy, J. R. (2018). Recharge processes and vertical transfer investi-
- 1114 gated through long-term monitoring of dissolved gases in shallow groundwater.
- 1115 *Journal of Hydrology*, 560, 275–288. doi: 10.1016/j.jhydrol.2018.02.077
- 1116 Montgomery, D. R., Dietrich, W. E., Torres, R., Anderson, S. P., Heffner, J. T.,
- 1117 & Loague, K. (1997). Hydrologic response of a steep, unchanneled valley
- 1118 to natural and applied rainfall. *Water Resour. Res.*, 33(1), 91–109. doi:
- 1119 10.1029/96WR02985
- 1120 Morgenstern, U., Stewart, M. K., & Stenger, R. (2010). Dating of streamwater using
- 1121 tritium in a post nuclear bomb pulse world: Continuous variation of mean
- 1122 transit time with streamflow. *Hydrol. Earth Syst. Sci.*, 14(11), 2289–2301. doi:
- 1123 10.5194/hess-14-2289-2010
- 1124 Mougin, B., Allier, D., Blanchin, R., Carn, A., Courtois, N., Gateau, C., ... Wyns,
- 1125 R. (2008). *SILURES Bretagne - Rapport final - Année 5* (Tech. Rep. No.
- 1126 RP-56457-FR). Retrieved from [http://infoterre.brgm.fr/rapports/](http://infoterre.brgm.fr/rapports/RP-56457-FR.pdf)
- 1127 [RP-56457-FR.pdf](http://infoterre.brgm.fr/rapports/RP-56457-FR.pdf)
- 1128 Mougin, B., Carn, A., Thomas, E., & Jégou, J.-P. (2002). *SILURES Bretagne Etat*
- 1129 *d'avancement de l'année 1* (Tech. Rep. No. RP-51481-FR). Retrieved from
- 1130 <http://infoterre.brgm.fr/rapports/RP-51481-FR.pdf>
- 1131 Mougin, B., Thomas, E., Mathieu, F., Baltassat, J.-M., Schroetter, J.-M., Blanchin,
- 1132 R., ... Lucassou, F. (2015). *Calcul des volumes d'eau souterraine sur 12*
- 1133 *bassins versants bretons en zone de socle et apports sur les temps moyens de*
- 1134 *résidence des eaux souterraines*. Retrieved from [https://hal-brgm.archives](https://hal-brgm.archives-ouvertes.fr/hal-01180210)
- 1135 [-ouvertes.fr/hal-01180210](https://hal-brgm.archives-ouvertes.fr/hal-01180210)
- 1136 Mougin, B., Thomas, E., Wyns, R., Blanchin, R., & Mathieu, F. (2004). *Qual-*
- 1137 *ité des eaux en Bretagne - Ruissellement - Infiltration - Temps de réponse.*
- 1138 *Bassins versants : Le Yar (Côtes d'Armor), l'Horn (Finistère), et du Coët-*
- 1139 *Dan (Morbihan)* (Tech. Rep. No. RP-52731-FR). BRGM. Retrieved from
- 1140 <http://infoterre.brgm.fr/rapports/RP-52731-FR.pdf>
- 1141 Musy, A., & Higy, C. (2004). *Hydrologie: Une science de la nature*. PPUR presses
- 1142 polytechniques.
- 1143 Nguyen, T. V., Kumar, R., Lutz, S. R., Musolff, A., Yang, J., & Fleckenstein, J. H.
- 1144 (2021). Modeling Nitrate Export From a Mesoscale Catchment Using Stor-
- 1145 Age Selection Functions. *Water Resour. Res.*, 57(2), e2020WR028490. doi:

- 1146 10.1029/2020WR028490
- 1147 Paniconi, C., & Putti, M. (2015). Physically based modeling in catchment hydrology  
1148 at 50: Survey and outlook: SURVEY OF PHYSICALLY BASED MODELING  
1149 IN CATCHMENT HYDROLOGY. *Water Resour. Res.*, *51*(9), 7090–7129. doi:  
1150 10.1002/2015WR017780
- 1151 Paniconi, C., Troch, P. A., van Loon, E. E., & Hilberts, A. G. J. (2003). Hillslope-  
1152 storage Boussinesq model for subsurface flow and variable source areas along  
1153 complex hillslopes: 2. Intercomparison with a three-dimensional Richards equa-  
1154 tion model. *Water Resour. Res.*, *39*(11), 1317. doi: 10.1029/2002WR001730
- 1155 Peters, N. E., Burns, D. A., & Aulenbach, B. T. (2014). Evaluation of High-  
1156 Frequency Mean Streamwater Transit-Time Estimates Using Groundwater  
1157 Age and Dissolved Silica Concentrations in a Small Forested Watershed. *Aquat*  
1158 *Geochem*, *20*(2-3), 183–202. doi: 10.1007/s10498-013-9207-6
- 1159 Pfankuch, H. (1963). Contribution à l'étude des déplacements de fluides miscibles  
1160 dans un milieu poreux. *Rev. Inst. Fr. Pet.*, *18*, 215–270.
- 1161 Pinay, G., Peiffer, S., Dreuzy, J.-R., Krause, S., Hannah, D. M., Fleckenstein, J. H.,  
1162 ... Hubert-Moy, L. (2015). Upscaling Nitrogen Removal Capacity from Lo-  
1163 cal Hotspots to Low Stream Orders' Drainage Basins. *Ecosystems*, *18*(6),  
1164 1101–1120. doi: 10.1007/s10021-015-9878-5
- 1165 Pollock, D. W. (1988). Semianalytical Computation of Path Lines for Finite-  
1166 Difference Models. *Ground Water*, *26*(6), 743–750. doi: 10.1111/j.1745-6584  
1167 .1988.tb00425.x
- 1168 Putti, M., & Paniconi, C. (2004). Time step and stability control for a coupled  
1169 model of surface and subsurface flow. In C. T. Miller & G. F. Pinder (Eds.),  
1170 *Developments in Water Science* (Vol. 55, pp. 1391–1402). Elsevier. doi: 10  
1171 .1016/S0167-5648(04)80152-7
- 1172 Quintana-Seguí, P., Le Moigne, P., Durand, Y., Martin, E., Habets, F., Baillon, M.,  
1173 ... Morel, S. (2008). Analysis of Near-Surface Atmospheric Variables: Validation  
1174 of the SAFRAN Analysis over France. *J. Appl. Meteor. Climatol.*, *47*(1),  
1175 92–107. doi: 10.1175/2007JAMC1636.1
- 1176 Rademacher, L. K., Clark, J. F., Clow David W., & Hudson G. Bryant. (2005).  
1177 Old groundwater influence on stream hydrochemistry and catchment response  
1178 times in a small Sierra Nevada catchment: Sagehen Creek, California. *Water*  
1179 *Resources Research*, *41*(2). doi: 10.1029/2003WR002805
- 1180 Rademacher, L. K., Clark, J. F., Hudson, G. B., Erman, D. C., & Erman, N. A.  
1181 (2001). Chemical evolution of shallow groundwater as recorded by springs,  
1182 Sagehen basin; Nevada County, California. *Chemical Geology*, *179*(1), 37–51.  
1183 doi: 10.1016/S0009-2541(01)00314-X
- 1184 Reggiani, P., & Schellekens, J. (2003). Modelling of hydrological responses: The  
1185 representative elementary watershed approach as an alternative blueprint  
1186 for watershed modelling. *Hydrol. Process.*, *17*(18), 3785–3789. doi:  
1187 10.1002/hyp.5167
- 1188 Reggiani, P., Sivapalan, M., & Majid Hassanizadeh, S. (1998). A unifying framework  
1189 for watershed thermodynamics: Balance equations for mass, momentum, en-  
1190 ergy and entropy, and the second law of thermodynamics. *Advances in Water*  
1191 *Resources*, *22*(4), 367–398. doi: 10.1016/S0309-1708(98)00012-8
- 1192 Remondi, F., Botter, M., Burlando, P., & Fatichi, S. (2019). Variability of transit  
1193 time distributions with climate and topography: A modelling approach. *Jour-*

- 1194 *nal of Hydrology*, 569, 37–50. doi: 10.1016/j.jhydrol.2018.11.011
- 1195 Remondi, F., Kirchner, J. W., Burlando, P., & Fatichi, S. (2018). Water Flux  
1196 Tracking With a Distributed Hydrological Model to Quantify Controls on the  
1197 Spatiotemporal Variability of Transit Time Distributions. *Water Resour. Res.*,  
1198 54(4), 3081–3099. doi: 10.1002/2017WR021689
- 1199 Rinaldo, A., Benettin, P., Harman, C. J., Hrachowitz, M., McGuire, K. J., van der  
1200 Velde, Y., . . . Botter, G. (2015). Storage selection functions: A coherent  
1201 framework for quantifying how catchments store and release water and solutes:  
1202 ON STORAGE SELECTION FUNCTIONS. *Water Resour. Res.*, 51(6),  
1203 4840–4847. doi: 10.1002/2015WR017273
- 1204 Rodriguez, N. B., & Klaus, J. (2019). Catchment Travel Times From Compos-  
1205 ite StorAge Selection Functions Representing the Superposition of Stream-  
1206 flow Generation Processes. *Water Resour. Res.*, 55(11), 9292–9314. doi:  
1207 10.1029/2019WR024973
- 1208 Rolle, M., Eberhardt, C., Chiogna, G., Cirpka, O. A., & Grathwohl, P. (2009).  
1209 Enhancement of dilution and transverse reactive mixing in porous media: Ex-  
1210 periments and model-based interpretation. *Journal of Contaminant Hydrology*,  
1211 110(3), 130–142. doi: 10.1016/j.jconhyd.2009.10.003
- 1212 Roques, C., Bour, O., Aquilina, L., Dewandel, B., Leray, S., Schroetter, J., . . . Mou-  
1213 gin, B. (2014). Hydrological behavior of a deep sub-vertical fault in crystalline  
1214 basement and relationships with surrounding reservoirs. *Journal of Hydrology*,  
1215 509, 42–54. doi: 10.1016/j.jhydrol.2013.11.023
- 1216 Scaini, A., Audebert, M., Hissler, C., Fenicia, F., Gourdol, L., Pfister, L., & Beven,  
1217 K. J. (2017). Velocity and celerity dynamics at plot scale inferred from ar-  
1218 tificial tracing experiments and time-lapse ERT. *Journal of Hydrology*, 546,  
1219 28–43. doi: 10.1016/j.jhydrol.2016.12.035
- 1220 Schwanghart, W., & Scherler, D. (2014). Short Communication: TopoToolbox 2  
1221 – MATLAB-based software for topographic analysis and modeling in Earth  
1222 surface sciences. *Earth Surf. Dynam.*, 2(1), 1–7. doi: 10.5194/esurf-2-1-2014
- 1223 Schwientek, M., Maloszewski, P., & Einsiedl, F. (2009). Effect of the unsat-  
1224 urated zone thickness on the distribution of water mean transit times in  
1225 a porous aquifer. *Journal of Hydrology*, 373(3), 516–526. doi: 10.1016/  
1226 j.jhydrol.2009.05.015
- 1227 Shampine, L., Reichelt, M., & Kierzenka, J. (1999). Solving Index-1 DAEs  
1228 in MATLAB and Simulink. *SIAM Rev.*, 41(3), 538–552. doi: 10.1137/  
1229 S003614459933425X
- 1230 Solder, J. E., Stolp, B. J., Heilweil, V. M., & Susong, D. D. (2016). Characterization  
1231 of mean transit time at large springs in the Upper Colorado River Basin, USA:  
1232 A tool for assessing groundwater discharge vulnerability. *Hydrogeol J*, 24(8),  
1233 2017–2033. doi: 10.1007/s10040-016-1440-9
- 1234 Sprenger, M., Stumpp, C., Weiler, M., Aeschbach, W., Allen, S. T., Benettin,  
1235 P., . . . Werner, C. (2019). The Demographics of Water: A Review of  
1236 Water Ages in the Critical Zone. *Rev. Geophys.*, 57(3), 800–834. doi:  
1237 10.1029/2018RG000633
- 1238 Stolp, B. J., Solomon, D. K., Suckow, A., Vitvar, T., Rank, D., Aggarwal, P. K., &  
1239 Han, L. F. (2010). Age dating base flow at springs and gaining streams using  
1240 helium-3 and tritium: Fische-Dagnitz system, southern Vienna Basin, Austria.  
1241 *Water Resour. Res.*, 46(7). doi: 10.1029/2009WR008006

- 1242 Strack, O. D. L. (1984). Three-Dimensional Streamlines in Dupuit-Forchheimer  
1243 Models. *Water Resour. Res.*, *20*(7), 812–822. doi: 10.1029/WR020i007p00812
- 1244 Suckow, A. (2014). The age of groundwater – Definitions, models and why we do not  
1245 need this term. *Applied Geochemistry*, *50*, 222–230. doi: 10.1016/j.apgeochem  
1246 .2014.04.016
- 1247 Therrien, R., & Sudicky, E. A. (1996). Three-dimensional analysis of variably-  
1248 saturated flow and solute transport in discretely-fractured porous me-  
1249 dia. *Journal of Contaminant Hydrology*, *23*(1), 1–44. doi: 10.1016/  
1250 0169-7722(95)00088-7
- 1251 Troch, P. A., Berne, A., Bogaart, P., Harman, C., Hilberts, A. G. J., Lyon, S. W.,  
1252 ... Verhoest, N. E. C. (2013). The importance of hydraulic groundwater theory in catchment hydrology: The legacy of Wilfried Brutsaert and Jean-Yves  
1253 Parlange. *Water Resour. Res.*, *49*(9), 5099–5116. doi: 10.1002/wrcr.20407
- 1254 Troch, P. A., Paniconi, C., & Emiel van Loon, E. (2003). Hillslope-storage Boussi-  
1255 nesq model for subsurface flow and variable source areas along complex hill-  
1256 slopes: 1. Formulation and characteristic response. *Water Resour. Res.*,  
1257 *39*(11), 1316. doi: 10.1029/2002WR001728
- 1258 Tromp-van Meerveld, H. J., & McDonnell, J. J. (2006). Threshold relations in sub-  
1259 surface stormflow: 2. The fill and spill hypothesis. *Water Resour. Res.*, *42*(2),  
1260 W02411. doi: 10.1029/2004WR003800
- 1261 Van Meter, K. J., & Basu, N. B. (2017). Time lags in watershed-scale nutrient trans-  
1262 port: An exploration of dominant controls. *Environ. Res. Lett.*, *12*(8), 084017.  
1263 doi: 10.1088/1748-9326/aa7bf4
- 1264 Van Meter, K. J., Basu, N. B., Veenstra, J. J., & Burras, C. L. (2016). The ni-  
1265 trogen legacy: Emerging evidence of nitrogen accumulation in anthropogenic  
1266 landscapes. *Environ. Res. Lett.*, *11*(3), 035014. doi: 10.1088/1748-9326/11/3/  
1267 035014
- 1268 Van Meter, K. J., Cappellen, P. V., & Basu, N. B. (2018). Legacy nitrogen may  
1269 prevent achievement of water quality goals in the Gulf of Mexico. *Science*,  
1270 *360*(6387), 427–430. doi: 10.1126/science.aar4462
- 1271 Vannier, O., Braud, I., & Anquetin, S. (2014). Regional estimation of catchment-  
1272 scale soil properties by means of streamflow recession analysis for use in dis-  
1273 tributed hydrological models. *Hydrological Processes*, *28*(26), 6276–6291. doi:  
1274 10.1002/hyp.10101
- 1275 Vautier, C., Abhervé, R., Labasque, T., Laverman, A. M., Guillou, A., Chatton, E.,  
1276 ... de Dreuzy, J.-R. (2020). Mapping gas exchanges in headwater streams  
1277 with membrane inlet mass spectrometry. *Journal of Hydrology*, *581*, 124398.  
1278 doi: 10.1016/j.jhydrol.2019.124398
- 1279 van der Velde, Y., de Rooij, G. H., Rozemeijer, J. C., van Geer, F. C., & Broers,  
1280 H. P. (2010). Nitrate response of a lowland catchment: On the relation be-  
1281 tween stream concentration and travel time distribution dynamics. *Water  
1282 Resour. Res.*, *46*(11), W11534. doi: 10.1029/2010WR009105
- 1283 van Verseveld, W. J., Barnard, H. R., Graham, C. B., McDonnell, J. J., Brooks,  
1284 J. R., & Weiler, M. (2017). A sprinkling experiment to quantify celer-  
1285 ity&ndash;velocity differences at the hillslope scale. *Hydrol. Earth Syst. Sci.*,  
1286 *21*(11), 5891–5910. doi: 10.5194/hess-21-5891-2017
- 1287 Vidal, J.-P., Martin, E., Franchistéguy, L., Baillon, M., & Soubeyroux, J.-M. (2010).  
1288 A 50-year high-resolution atmospheric reanalysis over France with the Safran  
1289

- 1290 system. *Int. J. Climatol.*, 30(11), 1627–1644. doi: 10.1002/joc.2003
- 1291 Visser, A., Thaw, M., Deinhart, A., Bibby, R., Safeeq, M., Conklin, M., ... Van der  
1292 Velde, Y. (2019). Cosmogenic Isotopes Unravel the Hydrochronology and  
1293 Water Storage Dynamics of the Southern Sierra Critical Zone. *Water Resour.  
1294 Res.*, 55(2), 1429–1450. doi: 10.1029/2018WR023665
- 1295 Vogel, J. C. (1967). Investigation of groundwater flow with radiocarbon. In *Isotopes  
1296 in hydrology. Proceedings of a symposium*. Retrieved from [http://inis.iaea  
1297 .org/Search/search.aspx?orig\\_q=RN:38061071](http://inis.iaea.org/Search/search.aspx?orig_q=RN:38061071)
- 1298 White, R. E., Wellings, S. R., & Bell, J. P. (1983). Seasonal variations in nitrate  
1299 leaching in structured clay soils under mixed land use. *Agricultural Water  
1300 Management*, 7(4), 391–410. doi: 10.1016/0378-3774(83)90030-6
- 1301 Wilson, C. J., & Dietrich, P. (1987). The contribution of bedrock groundwater flow  
1302 to storm runoff and high pore water pressure development in hollows. *IAHS  
1303 Publ.*, 165, 49-59.
- 1304 Wilusz, D. C., Harman, C. J., & Ball, W. P. (2017). Sensitivity of Catchment Tran-  
1305 sit Times to Rainfall Variability Under Present and Future Climates. *Water  
1306 Resour. Res.*, 53(12), 10231–10256. doi: 10.1002/2017WR020894
- 1307 Wilusz, D. C., Harman, C. J., Ball, W. P., Maxwell, R. M., & Buda, A. R. (2020).  
1308 Using Particle Tracking to Understand Flow Paths, Age Distributions,  
1309 and the Paradoxical Origins of the Inverse Storage Effect in an Experi-  
1310 mental Catchment. *Water Resour. Res.*, 56(4), e2019WR025140. doi:  
1311 10.1029/2019WR025140
- 1312 Wittenberg, H., & Sivapalan, M. (1999). Watershed groundwater balance estimation  
1313 using streamflow recession analysis and baseflow separation. *Journal of Hydrol-  
1314 ogy*, 219(1–2), 20–33. doi: 10.1016/S0022-1694(99)00040-2
- 1315 Yang, J., Heidbüchel, I., Musolff, A., Reinstorf, F., & Fleckenstein, J. H. (2018).  
1316 Exploring the Dynamics of Transit Times and Subsurface Mixing in a  
1317 Small Agricultural Catchment. *Water Resources Research*, 0(0). doi:  
1318 10.1002/2017WR021896
- 1319 Yang, X., Jomaa, S., Zink, M., Fleckenstein, J. H., Borchardt, D., & Rode, M.  
1320 (2018). A New Fully Distributed Model of Nitrate Transport and Re-  
1321 moval at Catchment Scale. *Water Resour. Res.*, 54(8), 5856–5877. doi:  
1322 10.1029/2017WR022380
- 1323 Zech, A., Attinger, S., Cvetkovic, V., Dagan, G., Dietrich, P., Fiori, A., ... Teutsch,  
1324 G. (2015). Is unique scaling of aquifer macrodispersivity supported by field  
1325 data? *Water Resour. Res.*, 51(9), 7662–7679. doi: 10.1002/2015WR017220